

# LANTHANIDE DOPED CRYSTALS FOR TUNABLE UV LASERS

Final Report

by

Richard MONCORGE

(march 1999)

United States Army

EUROPEAN RESEARCH OFFICE OF THE U.S. ARMY

London, England

CONTRACT NUMBER : N68171-97-M-5764

ISMRA/LABORATOIRE DE SPECTROSCOPIE ATOMIQUE-FRANCE

Approved for Public Release; distribution unlimited

19991004 058

The research reported in this document has been made possible through the support of the U.S. Government through its European Office of the U.S. Army.

**DTIC QUALITY INSPECTED 4**

## REPORT DOCUMENTATION PAGE

Form Approved

OMB No. 0704-0188

Public reporting burden for this collection of information is estimated to average 1 hour per response, including the time for reviewing instructions, searching existing data sources, gathering and maintaining the data needed, and completing and reviewing the collection of information. Send comments regarding this burden estimate or any other aspect of this collection of information, including suggestions for reducing this burden, to Washington Headquarters Services, Directorate for Information Operations and Reports, 1215 Jefferson Davis Highway, Suite 1204 Arlington, VA 22202-4302, and to the Office of Management and Budget, Paperwork Reduction Project (0704-0188), Washington, DC 20503.

1. AGENCY USE ONLY (Leave Blank)		2. REPORT DATE march 1999	3. REPORT TYPE AND DATES COVERED Final report	
4. TITLE AND SUBTITLE Lanthanide doped crystals for tunable UV lasers			5. FUNDING NUMBERS CN68171-97-M-5764	
6. AUTHOR(S) MONCORGE Richard				
7. PERFORMING ORGANIZATION NAME(S) AND ADDRESS(ES) ISMRA Laboratoire de Spectroscopie Atomique 6, Boulevard Maréchal Juin F-14050 CAEN Cedex 4 (FRANCE)			8. PERFORMING ORGANIZATION REPORT NUMBER	
9. SPONSORING/MONITORING AGENCY NAME(S) AND ADDRESS(ES) NAVAL REGIONAL CONTRACTING CENTER DETACHMENT LONDON, BLOCK 2, WING 11 DoE COMPLEX, EASTCOTE ROAD RUISLIP, MIDDLEX, UK, HA48BS Todd McKamey 0181-385-5373			10. SPONSORING/MONITORING AGENCY REPORT NUMBER	
11. SUPPLEMENTARY NOTES				
12. DISTRIBUTION/AVAILABILITY STATEMENT <del>This report is intended only for the internal management use of the contractor and US government.</del>			12b. DISTRIBUTION CODE	
13. ABSTRACT (Maximum 200 words)  Several Pr <sup>3+</sup> doped fluoride and oxide crystals, most of them being grown in our laboratory, are investigated here spectroscopically to examine their potential use for tunable UV laser systems. The study is both experimental and theoretical with emphasis on measurements of excited state absorption (ESA) spectra, in particular to evaluate the possibility to operate these laser systems after two-step excitations using visible/near-UV pump photons. The complex electronic structure (positions of the energy levels, polarizations of the transitions) of the first excited electronic configuration 4f5d for Pr <sup>3+</sup> (the one giving rise to UV emission) is clearly demonstrated. Assuming negligible ESA in the emitting level, which is probably too optimistic, simulations based on ESA and fluorescence data show the possibility of 20% laser gain per pass using moderate pump energies. It is then concluded and recommended to address more specifically the crystal growth question to obtain better quality materials and also to investigate new types of crystals, either doped with Pr <sup>3+</sup> , but emitting at slightly longer wavelengths, between about 260 and 310 nm, to reduce ESA in the emitting state, or doped with Nd <sup>3+</sup> to reach then UV emissions at shorter wavelengths.				
14. SUBJECT ITEMS			15. NUMBER OF PAGES 50	
			16. PRICE CODE	
17. SECURITY CLASSIFICATION OF REPORT	18. SECURITY CLASSIFICATION OF THIS PAGE	19. SECURITY CLASSIFICATION OF ABSTRACT	20. LIMITATION OF ABSTRACT	

N7 340-01-280-3300

Standard Form 298 (Rev. 2-89)  
Prescribed by ANSI Std. Z39-18  
298-102

## SUMMARY

Several  $\text{Pr}^{3+}$  doped fluoride and oxide crystals, most of them being grown in our laboratory, are investigated here spectroscopically to examine their potential use for tunable UV laser systems. The study is both experimental and theoretical with emphasis on measurements of excited state absorption (ESA) spectra, in particular to evaluate the possibility to operate these laser systems after two-step excitations using visible/near-UV pump photons. The complex electronic structure (positions of the energy levels, polarizations of the transitions) of the first excited electronic configuration  $4f5d$  for  $\text{Pr}^{3+}$  (the one giving rise to UV emission) is clearly demonstrated. Assuming negligible ESA in the emitting level, which is probably too optimistic, simulations based on ESA and fluorescence data show the possibility of 20% laser gain per pass using moderate pump energies. It is then concluded and recommended to address more specifically the crystal growth question to obtain better quality materials and also to investigate new types of crystals, either doped with  $\text{Pr}^{3+}$ , but emitting at slightly longer wavelengths, between about 260 and 310 nm, to reduce ESA in the emitting state, or doped with  $\text{Nd}^{3+}$  to reach then UV emissions at shorter wavelengths.

### List of Keywords:

Praseodymium, crystal, laser, excited-state-absorption, ultraviolet, neodymium

### List of publications:

"Spectroscopic investigation of the  $4f5d$  energy levels of  $\text{Pr}^{3+}$  in fluoride crystals via excited-state absorption and two-step excitation measurements" M. Laroche, A. Braud, S. Girard, J.L. Doualan, R. Moncorgé, M. Thuau, L.D. Merkle; J. Opt. Soc. Am. To appear (1999)

" $4f^2$  to  $4f5d$  excited-state absorption in  $\text{Pr}^{3+}:\text{YAlO}_3$ " S. Nicolas, M. Laroche, S. Girard, R. Moncorgé, Y. Guyot, M.F. Joubert, E. Descroix, A.G. Petrosyan"; J. Phys. Cond. Matter to appear (1999)

"UV-visible lasers based on Rare-earth ions" R. Moncorgé, J.D. Merkle, B. Zandi; Mat. Res. Bull. to appear (1999)

## TABLE OF CONTENTS

	Page
<b>Statement of Work</b>	
1. Scope	1
2. Objectives	2
<b>Results and Discussion of the Results</b>	
1. Materials considered and selected	2
2. Absorption/Fluorescence of the materials	3
3. Excited state absorption (ESA) data	6
A. ESA experimental conditions	6
B. ESA experimental results	8
C. Energy level analysis	11
4. Excited-state excitation and two-step pumping model:	13
5. Tentative gain measurements	15
6. Solarisation experiments	15
<b>Conclusions and Recommendations</b>	17
<b>Literature Cited</b>	20
<b>Figures</b>	22

# LANTHANIDE DOPED CRYSTALS FOR TUNABLE UV LASERS

Final Report  
by

Richard MONCORGE  
(march 1999)

## STATEMENT OF WORK

### 1. Scope :

Conduct a **fundamental study** of the optical properties of rare earth doped crystals towards their use as laser materials.

Attention is mainly addressed to the study of crystals doped with  $\text{Pr}^{3+}$  (praseodymium) ions presenting near UV emission bands associated with  $4f5d \rightarrow 4f^2$  interconfigurational transitions because of their potential for tunable UV laser systems.  $\text{Pr}^{3+}$  is also a very attractive ion because it can give rise, depending on the host materials, to many emission transitions between 400 and 700 nm and because its high energy levels are sufficiently far apart from each other to allow good fluorescence quantum efficiencies.

Investigations concentrated initially on crystals already available to us, including  $\text{YAlO}_3$ ,  $\text{GdAlO}_3$ ,  $\text{Ca}_5(\text{PO}_4)_3\text{F}$  and  $\text{Sr}_5(\text{PO}_4)_3\text{F}$ . The aluminates, with the perovskite structure, have already exhibited favorable visible laser properties for Pr [1]. The phosphates, with the apatite structure, are successful laser hosts for other rare earth ions [2], and spectroscopy which we have undertaken for other purposes provided a good start on the present study. As the study progressed, we have added further samples as needed, oxides such as the non-linear material YCOB ( $\text{YCa}_4\text{B}_3\text{O}_{10}$ ) but mainly fluorides such as  $\text{LiYF}_4$ ,  $\text{LiLuF}_4$ ,  $\text{BaY}_2\text{F}_8$ ,  $\text{KY}_3\text{F}_{10}$  and  $\text{KYF}_4$  utilizing our Czochralski growth facility in Caen

The study is both experimental and theoretical with emphasis on measurements of absorption spectra in the excited states (ESA) of the luminescent ions and assignments/predictions of the various optical transitions. The ESA measurements are used to predict the various dynamical processes which can be involved to operate these laser systems in the UV domain after two-step excitations using visible/near-UV pump photons. They also serve afterwards, along with literature data, as a basis for the discussion of the UV laser potential of other ions such as  $\text{Nd}^{3+}$ .

## 2. Objectives :

Semiconductor laser diodes are being studied to realize compact laser systems working at various wavelengths. This work is intended to explore the possibility of exciting broadband UV emissions of rare earth ions with the aid of solid-state visible/near-UV sources instead of the customary pumping with UV radiations such as that of excimer lasers. In particular, this is expected to be less detrimental for the laser material and avoid the solarization (coloration) problems.

An additional objective was to establish co-operative working relationships with Army researchers.

## RESULTS and DISCUSSION OF THE RESULTS

### 1. Materials considered and selected :

Basic spectroscopy measurements such as registration of ground-state absorption (GSA) spectra and of UV fluorescence following UV excitation allowed us first to select a restricted number of materials among those which were initially considered (see in First Technical Letter Report).

Rejected materials :

- Perovskite  $\text{Pr:GdAlO}_3$  was eliminated because the  $4f5d \rightarrow 4f^2$  inter-configurational UV luminescence of  $\text{Pr}^{3+}$  in this material is quenched due to  $\text{Pr}^{3+} \rightarrow \text{Gd}^{3+}$  energy transfers
- Fluoro-apatites  $\text{Pr:Ca}_5(\text{PO}_4)_3\text{F}$  and  $\text{Sr}_5(\text{PO}_4)\text{F}$  were eliminated because no UV fluorescence was observed either; in this case, the onset for UV absorption is probably low enough to allow

non-radiative relaxations to occur between the energy levels of the  $4f5d$  and  $4f^2$  electronic configurations. Following Ref. 3, these non-radiative relaxations are strongly favored in case of large Stokes shifts between the energy levels, and this generally occurs in materials in which the dopant ion occupies a site with a large coordination number, a « spacy site »

- Pr:YCOB ( $\text{YCa}_4\text{B}_3\text{O}_{10}$ ) was rejected for the same reasons as the fluoro-apatites; moreover, in this system, the borate groupments lead to high phonon energies, thus favor non-radiative multiphonon relaxations even more efficiently

The materials retained for more extensive investigations were:

- Perovskite Pr:YAlO<sub>3</sub>, because good quality crystals with various dopant concentrations (0.1, 0.5, 1 and 3 at.%) were already available in the laboratory and because larger and improved quality samples can be obtained from other crystal growers with whom we collaborate very closely

- Fluorides Pr:LiYF<sub>4</sub>, LiLuF<sub>4</sub>, BaY<sub>2</sub>F<sub>8</sub>, KY<sub>3</sub>F<sub>10</sub> and KYF<sub>4</sub>, because some of them were already available in the laboratory but also because we decided to grow these crystals ourselves to have more flexibility

The selected crystals were all good quality crystals, at least for the spectroscopic measurements. **Significant improvements were obtained in the crystal growth** of our fluorides by changing the purification process of the raw materials and by mounting a specially dedicated fluorination oven to avoid any trace of oxygen. The size of the spectroscopic samples was of the order of  $5 \times 5 \times 3 \text{ mm}^3$ , with dopant concentrations, in the case of fluorides, of about 0.5 at%.

## 2. Absorption/fluorescence properties of the materials :

Though very few data can be found in the case of Pr :KY<sub>3</sub>F<sub>10</sub> and KYF<sub>4</sub>, most of the basic optical properties of the other selected materials were already reported in the literature.

Concerning Pr<sup>3+</sup>-doped yttrium orthoaluminate YAlO<sub>3</sub>, the energy levels of the Pr<sup>3+</sup>  $4f^2$  ground configuration are well known [4]. The seven lower manifolds are located in the infrared range; the five <sup>1</sup>D<sub>2</sub> Stark components are between 16380 and 17040 cm<sup>-1</sup>, then the <sup>3</sup>P<sub>0,1,2</sub> and <sup>1</sup>I<sub>6</sub> states are in the 20420-22420 cm<sup>-1</sup> spectral domain. The emission spectrum of the  $4f5d$  first excited configuration exhibits two broad bands at room temperature centred at 247 and 282 nm [5,6] which are due to

transitions originating from the lowest 4f5d level and terminating on the  $^3H_4$  and  $^3F_4$  manifolds of the 4f<sup>2</sup> configuration. Their excitation spectrum exhibits, at energies below the band gap energy (8 eV [7,8]), two groups of bands, located around 46080 and 55550 cm<sup>-1</sup> respectively, assigned to the 4f<sup>2</sup> → 4f5d transitions [5].

The basic luminescence properties of **Pr :LiYF<sub>4</sub>** (4f<sup>2</sup> energy level positions and intraconfigurational transition intensities) can be found in Refs.9-11. Concerning the 4f<sup>2</sup>-4f5d optical transitions, unpolarized data were reported in Refs. 12 and 13. In the case of **Pr :BaY<sub>2</sub>F<sub>8</sub>**, 4f<sup>2</sup> luminescence and stimulated emission data were reported in Refs. 14 and 15 and 4f<sup>2</sup>-4f5d unpolarized spectra in Refs 12 and 16. As to **Pr :KY<sub>3</sub>F<sub>10</sub>**, the only report we are aware of is a HDL report of 1980 [17] which only gives the positions of the 4f<sup>2</sup> energy levels. Nothing was reported to our knowledge on the optical transitions between the 4f<sup>2</sup> and 4f5d configurations.

In the end, in the case of **Pr:KYF<sub>4</sub>**, nothing was found on the positions of the 4f<sup>2</sup> energy levels, and as for **Pr:KY<sub>3</sub>F<sub>10</sub>**, on its optical transitions between 4f<sup>2</sup> and 4f5d configurations.

Consequently, polarized ground state absorption (GSA) spectra were recorded again first to have more precise information about the real absorption of our crystals and more particularly in the blue and the orange spectral domains corresponding to the  $^3H_4 \rightarrow (^3P_{0,1,2}, ^1I_6)$  and  $^1D_2$  optical transitions since they will constitute the first pumping step of our excited-state absorption (ESA) and excited-state excitation (ESE) measurements. These polarized GSA spectra were registered by using a conventional Lambda 9 Perkin Elmer spectrometer and Glan-Thomson polarizers. We have reported these spectra in the Figures 1, 2, 3 and 4. In the case of the **Pr:LiYF<sub>4</sub>** and **Pr :KYF<sub>4</sub>** uniaxial crystals, the spectra had to be recorded with polarization parallel ( $\pi$ ) and perpendicular ( $\sigma$ ) to the crystallographic axis c. In the case of the biaxial crystals **Pr:YAlO<sub>3</sub>** and **Pr:BaY<sub>2</sub>F<sub>8</sub>** the spectra had to be recorded with polarization parallel to each of the three principal crystallographic axes, a, b and c, with a = 5.32 Å, b = 7.37 Å and c = 5.13 Å for YAlO<sub>3</sub> [19], and E//1, E//2 and E//3 (nomenclature used in Ref.18) for BaY<sub>2</sub>F<sub>8</sub>.

We also report in the Figures 5, 6 and 7 the 4f5d→4f<sup>2</sup> UV emission spectra (corrected from the spectral response of our experimental set-up) for the different systems. These spectra do not significantly depend on polarization so that no polarization is specified.

We finally anticipated on the discussion of the ESA results which will be reported in the next section by adding a figure (Fig. 8) on the energy level scheme of Pr :LiYF<sub>4</sub> to show the relative positions of the relevant 4f<sup>2</sup> and 4f5d configuration states. These energy level scheme shows that two-step excitation of the 4f5d states using visible and near UV photons should be possible in LiYF<sub>4</sub>:Pr<sup>3+</sup> (and in the other systems too).

As shown in the Figures 1 to 4, because of spin selection rule, the oscillator strength for the ground state absorption (GSA) transition to the (<sup>3</sup>P<sub>0,1,2</sub>, <sup>1</sup>I<sub>6</sub>) manifold, and more particularly that corresponding to the <sup>3</sup>H<sub>4</sub>→<sup>3</sup>P<sub>2</sub> transition around 450 nm, is significantly larger than that associated with the <sup>3</sup>H<sub>4</sub>→<sup>1</sup>D<sub>2</sub> transition around 600 nm. This is the reason why (but also because of reduced non-radiative multiphonon relaxations) the lifetime of the fluorescences coming from this <sup>1</sup>D<sub>2</sub> singlet state is always significantly longer than that coming from the emitting triplet state <sup>3</sup>P<sub>0</sub>. The positions of the <sup>1</sup>D<sub>2</sub> and <sup>3</sup>P<sub>0</sub> energy levels and their fluorescence lifetimes measured at room temperature are reported in Table 1. Consequently, absorption in the triplet state is more efficient but more energy can be stored into the singlet so that both metastable levels can be interesting as intermediate states in the two-step pumping process mentioned above.

Materials	Pr :YAlO <sub>3</sub>	Pr :KY <sub>3</sub> F <sub>10</sub>	Pr :LiYF <sub>4</sub>	Pr :BaY <sub>2</sub> F <sub>8</sub>	Pr :KYF <sub>4</sub>
v( <sup>3</sup> P <sub>0</sub> )	20410 cm <sup>-1</sup>	20730 cm <sup>-1</sup>	20860 cm <sup>-1</sup>	20840 cm <sup>-1</sup>	21000 cm <sup>-1</sup>
τ( <sup>3</sup> P <sub>0</sub> )	11 μs	33.5 μs	43.5 μs	42.5 μs	63 μs
v( <sup>1</sup> D <sub>2</sub> )	16380 cm <sup>-1</sup>	16670 cm <sup>-1</sup>	16740 cm <sup>-1</sup>	16650 cm <sup>-1</sup>	17540 cm <sup>-1</sup>
τ( <sup>1</sup> D <sub>2</sub> )	165 μs	92.5 μs	205 μs	175 μs	300 μs

Table 1 : Approximate positions and fluorescence lifetimes of the <sup>1</sup>D<sub>2</sub> and <sup>3</sup>P<sub>0</sub> metastable levels in Pr doped YAlO<sub>3</sub>, KY<sub>3</sub>F<sub>10</sub>, YLiF<sub>4</sub>, BaY<sub>2</sub>F<sub>8</sub> and KYF<sub>4</sub>

On the other hand, as shown in the Figures 5 to 7, except for Pr :KY<sub>3</sub>F<sub>10</sub>, all the UV emission bands have about the same profiles, that of two bands, the shorter wavelength one being more intense than the other. The spectra of Pr :LiYF<sub>4</sub> and Pr :BaY<sub>2</sub>F<sub>8</sub> both extend from about 220 to 280 nm, the former being more structured than the latter. The spectrum of Pr :YAlO<sub>3</sub> is very similar to that of Pr:BaY<sub>2</sub>F<sub>8</sub> but shifted to slightly longer wavelengths, extending from 240 to 310 nm. The emission spectrum of Pr:KY<sub>3</sub>F<sub>10</sub> is substantially different. The bands are much broader than in the other systems, the one at

the longer wavelengths is the more intense and the spectrum extends from about 220 to 320 nm which is very interesting for broad laser wavelength tunability.

### 3. Excited-state absorption (ESA) data :

These measurements were made, as mentioned in the beginning, to evaluate the UV laser potential of the different Pr doped crystals following two-step excitations using visible/near UV pump photons. The first step consists in bringing the Pr ions into one of their  $^1D_2$  or  $^3P_{0,1,2}$  metastable levels and the second one in bringing the ions in these levels into the 4f5d broad band.

#### A. ESA experimental conditions :

ESA measurements were performed by using the pump-probe experimental set-up shown in Figure 9. The pump source was provided by a **broad-band optical parametric oscillator** (OPO GWU model C355) widely tunable in the visible and infrared domains. It is pumped by the third harmonic of a Q-switched Nd :YAG laser (Spectron model 404G) and emits nearly 10 mJ per pulse with a pulse duration of 4-5 nsec at a repetition rate of 10 Hz. The output wavelength of the signal wave was tuned either around 450-480 nm ( $^3H_4 \rightarrow ^3P_J$ ,  $^1I_6$ ) or around 590 nm ( $^3H_4 \rightarrow ^1D_2$ ). The pump beam diameter on the sample was adjusted with a  $f = 22$  cm focal length lens and was limited to a value of 500  $\mu\text{m}$  with the aid of a small aperture on the crystal mount. The pulse energy of the pump beam passing through this aperture was reduced to less than one mJ to avoid any optical damage and the pump fluence was typically of the order of 0.15 to 0.25 J/cm<sup>2</sup>. The probe beam was provided by a continuous wave (CW) high pressure **Xe arc-lamp** (Osram 100W). We finally used a Xe lamp, instead of a deuterium lamp (as was reported in our « Second Technical Report Letter) because the smaller size of the emitting element allowed a better focusing inside the crystal. Another improvement was brought by collimating and focusing the probe light with the aid of concave **mirrors instead of lenses**; by this way, we could get rid of the chromaticity problems we had and could collect more light onto the detector. The probe light propagated colinearly to the pump beam through the sample and it was collimated and focused successively onto the sample and the entrance slit of a monochromator thanks to these mirrors. The probe beam was spectrally analysed with a  $\frac{1}{4}$  m Oriel monochromator (model 77200) equipped with a 600 gr/mm grating blazed at 200 nm. The detection system consisted of a photomultiplier tube

(Hamamatsu model R3896 with a photocathode extended into the UV), a fast digitized oscilloscope (Tektronix TDS 350) and a boxcar integrator (PAR model 162) interfaced to a PC computer.

The ESA spectra could be recorded from 450 down to 220 nm. Below 220 nm, ESA measurements were not possible because of direct  $4f^2(^3H_4) \rightarrow 4f5d$  absorption. Polarized ESA spectra were recorded with the aid of a Glan Taylor prism made of  $\alpha$ -BBO especially designed for the UV spectral domain between 200 and 400 nm. These ESA spectra were calibrated in the following way :

When the pump beam was switched-off, the only populated multiplet is the ground state multiplet  $^3H_4$  and the population density is  $N_T$ , the chemically measured  $Pr^{3+}$  dopant concentration inside the crystals. The probe beam intensity transmitted throughout the sample in this unpumped case noted  $I_u$  is then given by the Beer-Lambert's law for small beam incident intensities  $I_0$ :

$$I_u = I_0 \exp(-N_T \sigma_{GSA}(\lambda)l) \quad (1)$$

$\sigma_{GSA}$  is the ground state absorption (GSA) cross section and  $l$  the length of the sample. When the crystal is pumped and if the probe beam intensity is measured immediately after the pump pulse (by opening the gate of the boxcar a few microseconds after this pump pulse), the only populated excited level is the one directly excited, i.e. (depending on the selected pump wavelength) the  $^3P_0$  or the  $^1D_2$  level in the present situation. So, if  $N^*$  stands for the population density in this excited level, the probe beam intensity  $I_p$  in this pumped case then becomes:

$$I_p = I_0 \exp\left(-\left(N_T - N^*\right)\sigma_{GSA}(\lambda)l + N^*\sigma_{SE}(\lambda)l - N^*\sigma_{ESA}(\lambda)l\right) \quad (2)$$

Here the subscript "p" indicates the pumped case,  $\sigma_{SE}$  is the stimulated emission (SE) cross section and  $\sigma_{ESA}$  is the ESA cross section. Then, Equations (1) and (2) can be combined to obtain :

$$\sigma_{ESA}(\lambda) - \sigma_{SE}(\lambda) - \sigma_{GSA}(\lambda) = \frac{1}{N^*l} \ln\left(\frac{I_u}{I_p}\right) \quad (3)$$

In Pr doped fluoride crystals, the stimulated emission and the ground-state absorption cross sections are nil for wavelengths between  $\lambda \approx 220$  nm and  $\lambda \approx 450$  nm, and therefore the excited-state absorption cross section starting from the metastable level is the only term remaining in the expression (3).  $\sigma_{ESA}$  can be found just by writing :

$$\sigma_{\text{ESA}}(\lambda) = -\frac{1}{N^* I} \ln \left( 1 - \frac{\Delta I}{I_u} \right) \quad (4)$$

Here  $\Delta I = I_u - I_p$  stands for the intensity change of the probe beam.

Calibration of the recorded spectra ( $\Delta I(\lambda)$  and  $I_u(\lambda)$ ) therefore needs some experimental determination of the population density  $N^*$ . This can be done from the direct measurement of the absorbed excitation energy in the pumped and probed portion of the sample. For that purpose, pump energy is measured successively before and after the samples and for Pr doped and undoped crystals, to account for the Fresnel as well as the scattering losses, both effects becoming quite important in the UV domain. If we denote  $E_{\text{abs}}$  the measured absorbed energy, the excited-state ion density can be obtained by using the expression :

$$N^* = \frac{E_{\text{abs}} \lambda_p}{hcSI} \quad (5)$$

where  $S$  is the area of the small hole drilled into the crystal mount,  $h$  is the Planck's constant,  $c$  the speed of light and  $\lambda_p$  the pump wavelength. This calibration method is further checked by measuring the bleaching effect experienced by the GSA transition  $^3H_4 \rightarrow ^3P_J$  after direct pumping into level  $^1D_2$ . The absorption line strength associated with the  $^3H_4 \rightarrow ^3P_2$  transition of the  $\text{Pr}^{3+}$  ion is the strongest one and thus is particularly useful to detect small variations in the ground state population after optical pumping.

## B. ESA experimental results

The polarized ESA spectra recorded after excitation into the  $^3P_J$ ,  $^1I_6$  and  $^1D_2$  levels for the five different crystals investigated here are presented in the Figures 10 to 14. These spectra are reported in units of wavenumbers ( $\text{cm}^{-1}$ ) and have been shifted by the energies of the respective  $^3P_0$  and  $^1D_2$  absorbing excited levels (see in Table 1) by using the expressions

$$\begin{aligned} \bar{\nu}(4f5d) &= \bar{\nu}(^3P_0) + \bar{\nu}(^3P_0 \rightarrow 4f5d) \\ \text{and } \bar{\nu}(4f5d) &= \bar{\nu}(^1D_2) + \bar{\nu}(^1D_2 \rightarrow 4f5d) \end{aligned} \quad (6)$$

to give the real positions of the 4f5d energy levels.

The pump wavelength was adjusted for each system by optimizing the fluorescence intensity coming from these metastable levels ( $^3P_0$  and/or  $^1D_2$ ) down to the  $^3H_4$  ground state.  $KY_3F_{10}$  is cubic,  $LiYF_4$  and  $KYF_4$  are uniaxial and  $YAlO_3$  and  $BaY_2F_8$  are biaxial, so that the ESA spectra were recorded either with an unpolarized probe beam or with a probe beam polarized along or perpendicular to the principal axis or parallel to the three principal axes of the optical indicatrix, respectively.

As can be seen in Figures 10 to 14, the ESA cross sections are of the order of  $10^{-18} \text{ cm}^2$  which is typical for 4f-5d parity-allowed electric dipole transitions (see for example the absorption cross section of  $Ce^{3+}$  ions in  $LiCa(Sr)AlF_6$  [20]).

Concerning first Pr:KY<sub>3</sub>F<sub>10</sub>, there is no available data in the literature on the absorption bands characterizing the  $^3H_4 \rightarrow 4f5d$  transitions. In the case of Pr:KY<sub>3</sub>F<sub>10</sub>, according to our near UV absorption spectra, UV absorption rises rapidly at about 230 nm which corresponds to an energy of about  $43500 \text{ cm}^{-1}$ . This well coincides with the onset of the  $^3H_4 \rightarrow 4f5d$  absorption band deduced from the ESA spectra associated with the  $^3P_0 \rightarrow 4f5d$  and the  $^1D_2 \rightarrow 4f5d$  transitions and reported in Fig. 10. According to these spectra, the 4f5d electronic configuration splits in various components with a more or less pronounced spin character (spin selection rules for transitions starting from  $^3P_0$  or  $^1D_2$ ). The  $^3P_0 \rightarrow 4f5d$  ESA spectrum probably indicates at least four bands peaking around 210 nm ( $47500 \text{ cm}^{-1}$ ), 198 nm ( $50500 \text{ cm}^{-1}$ ), 188 nm ( $53000 \text{ cm}^{-1}$ ) and 182 nm ( $55000 \text{ cm}^{-1}$ ). The  $^1D_2 \rightarrow 4f5d$  ESA spectrum leads to five bands peaking around 215 nm ( $46500 \text{ cm}^{-1}$ ), 205 nm ( $48700 \text{ cm}^{-1}$ ), 195 nm ( $51200 \text{ cm}^{-1}$ ), 187 nm ( $53500 \text{ cm}^{-1}$ ), and 177 nm ( $56500 \text{ cm}^{-1}$ ). It is worth noting that both sets of energy levels are clearly distinct and that the lowest 4f5d energy level would be predominantly a spin singlet. For sake of clarity, we have reported the positions of these energy levels in Fig. 15.

In the case of Pr:LiYF<sub>4</sub> and Pr:BaY<sub>2</sub>F<sub>8</sub>, absorption/excitation spectra corresponding to the ground state absorption transition  $^3H_4 \rightarrow 4f5d$  were already reported in the literature [22,23] and [16], respectively. These unpolarized spectra were recorded up to  $70000 \text{ cm}^{-1}$  and are made of two groups of bands, two well resolved and separated broad absorption bands around  $47000$  and  $54000 \text{ cm}^{-1}$  and three overlapping ones between about  $60000$  and  $67000 \text{ cm}^{-1}$ . According to Ref. 16, these bands result from the crystal field splitting of the 4f5d electronic configuration into a well resolved orbital doublet and a triplet, respectively.

Concerning that aspect, one can also refer to the case of  $\text{Pr}:\text{LiLuF}_4$ , an isomorphic system of  $\text{LiYF}_4$ , for which a very clear absorption spectrum is reported in Ref. 24. It is worth noting that similar band-splittings could be observed, for example in the case of  $\text{BaY}_2\text{F}_8$  [16], with  $\text{Ce}^{3+}$  (5d),  $\text{Pr}^{3+}$  (4f5d) and  $\text{Nd}^{3+}$  (4f<sup>2</sup>5d) as well, indicating the predominant effect of the crystal field on the 5d orbitals. These UV ground state absorption/excitation bands do not show any really distinct fine structures (at least at room temperature) which could be assigned to the 4f-5d electrostatic interaction and/or the spin-orbit coupling. Our ESA spectra (Figs 11 and 12) for  $\text{Pr}:\text{YLiF}_4$  and  $\text{Pr}:\text{BaY}_2\text{F}_8$ , as well as for  $\text{Pr}:\text{KY}_3\text{F}_{10}$ , however, look more complex - and thus more informative. Indeed, these spectra are recorded in a more restricted domain, between 240 nm (41500  $\text{cm}^{-1}$ ) and 420 nm (23800  $\text{cm}^{-1}$ ), which corresponds to 4f5d energy levels between about 62500  $\text{cm}^{-1}$  (160 nm) and 44000  $\text{cm}^{-1}$  (224 nm), thus to energy levels associated with the above mentioned doublet. Also, they are polarized spectra (E//c or  $\sigma$ , E/c or  $\pi$  for  $\text{LiYF}_4$ , E//1, E//2 and E//3 for  $\text{BaY}_2\text{F}_8$  and they correspond to transitions from spin-singlet and spin-triplet states  $^1\text{D}_2$  and  $^3\text{P}_0$ , instead of from the only ground state triplet  $^3\text{H}_4$ .

In the case of  $\text{Pr}:\text{LiYF}_4$ , the  $^3\text{P}_0 \rightarrow 4\text{f}5\text{d}$  ESA spectrum (shifted by 20860  $\text{cm}^{-1}$ , the energy of the  $^3\text{P}_0$  absorbing state) consists of at least two groups of bands, one with peaks around 208 nm (48000  $\text{cm}^{-1}$ ) and 250 nm (50000  $\text{cm}^{-1}$ ), and the other around 190 nm (52500  $\text{cm}^{-1}$ ) and 180 nm (55500  $\text{cm}^{-1}$ ). As to the  $^1\text{D}_2 \rightarrow 4\text{f}5\text{d}$  ESA spectrum, it also consists of two groups of bands around 213 nm (47000  $\text{cm}^{-1}$ ) and 202 nm (49500  $\text{cm}^{-1}$ ), and at about 188, 183 and 175 nm (53000, 54500 and 57000  $\text{cm}^{-1}$ , respectively). As above, the corresponding 4f5d energy levels are reported in Fig. 15. According to these results, the lowest level of the 4f5d configuration might have a more pronounced spin-singlet character.

In the case of  $\text{Pr}:\text{BaY}_2\text{F}_8$ , for which the UV ground state absorption spectrum can be found in Ref. 16, similar results are obtained and the resulting 4f5d energy level positions are also reported in Fig. 15 (positions determined again, as above, by shifting the ESA spectra by the energies of the  $^3\text{P}_0$  and  $^1\text{D}_2$  absorbing states). As in the case of  $\text{Pr}:\text{LiYF}_4$  and  $\text{Pr}:\text{KY}_3\text{F}_{10}$ , the lowest level of the 4f5d configuration in  $\text{Pr}:\text{BaY}_2\text{F}_8$  would have a stronger spin-singlet character.

Concerning  $\text{Pr}:\text{YAlO}_3$ , the ESA spectra from the  $^3\text{P}_{0,1,2}$ ,  $^1\text{I}_6$  and  $^1\text{D}_2$  multiplets to the 4f5d band have been recorded between about 240 and 425 nm (23500 and 42000  $\text{cm}^{-1}$ ) which lead, after being shifted by the energies of these absorbing states (energies reported in the Table 1), to the spectra reported in

Fig. 13. As in the other systems, these spectra are strongly polarized and those corresponding to the  $^3P_{0,1,2}, ^1I_6 \rightarrow 4f5d$  ESA transition are very different from those associated with the  $^1D_2 \rightarrow 4f5d$ . According to these spectra, the probed 4f5d energy levels would lie in a frequency (spectral) domain going from about 44000 to 62000  $\text{cm}^{-1}$  (160 to 230 nm). According to Ref. 6, which gives the ground-state excitation spectrum of the 4f5d band obtained by using the synchrotron radiation, the totality of the energy levels then would lie within this frequency domain, the two groups of excitation bands which were clearly observed around 46000 and 57000  $\text{cm}^{-1}$  (217 and 175 nm), though certainly poorly resolved, being tentatively assigned to the cubic crystal field splitting with a value of about 11000  $\text{cm}^{-1}$ .

The ESA spectra of Pr:KYF<sub>4</sub> were recorded from the  $^3P_{0,1,2}, ^1I_6$  multiplets essentially, between about 270 and 420 nm (36000-24000  $\text{cm}^{-1}$ ). They are reported in Fig. 14, shifted by the energy of the  $^3P_0$  level which is given in Table 1. As can be seen from Fig. 13, the spectra do not seem as strongly polarized as in the other non-cubic systems.

### C. Energy level analysis :

From Fig. 15, it is clear that the observed ESA transitions end on 4f5d energy levels. According to Ref. 16, in the case of Pr:BaY<sub>2</sub>F<sub>8</sub>, between about 45000 and 58000  $\text{cm}^{-1}$ , these transitions would end on the two lowest and well separated components of the 4f5d electronic configuration which appear in the ground state absorption spectra. These components might be due to the effect of the local tetragonal crystal field distortion on the low energy E component resulting itself from the cubic splitting of the 5d electronic orbitals, so in fact to only a part, the low energy portion, of the 4f5d energy levels. This situation occurs in all the fluorides investigated here in LiYF<sub>4</sub> and BaY<sub>2</sub>F<sub>8</sub> for sure, and probably also in KY<sub>3</sub>F<sub>10</sub> and KYF<sub>4</sub>. This is different in the case of Pr:YAP (see in Fig. 16). In this system, indeed, our ESA spectra probably cover the entire 4f5d band.

Now, the question arises concerning the identity of the various components appearing in the ESA spectra. According to several authors (see in Refs 25, 26 for example), the crystal field effect can be so large compared to that experienced by the 4f electron and compared to the electrostatic interaction between the 4f and 5d electrons, that the 4f and the 5d electrons can be considered as separate systems. In this hypothesis, the mixed states can be constructed from the

separate states of the 4f and the 5d electrons within the crystal. Since in all the investigated crystals, the  $\text{Pr}^{3+}$  ions substitute for  $\text{Y}^{3+}$  ions in tetragonally distorted cubic sites ( $C_{4v}$ ,  $S_4$  (or  $D_{2d}$ ),  $C_2$  and  $C_s$  symmetry in the case of  $\text{KY}_3\text{F}_{10}$ ,  $\text{LiYF}_4$ ,  $\text{BaY}_2\text{F}_8$  and  $\text{YAlO}_3$ , respectively), the 5d orbitals split first, in  $T_d$  symmetry, into two, E and  $T_2$ , E being lower. Then the E orbitals split into two and the  $T_2$  orbitals split into two or three components depending on the local distortion. This interpretation is, however, very questionable since the local symmetry, in particular in the case of  $\text{BaY}_2\text{F}_8$  ( $C_2$ ) and  $\text{YAlO}_3$  ( $C_s$ ), is very low. For example, if we refer to the case of  $\text{Ce:YAlO}_3$  studied in the past by M.J. Weber [30], the 5d band split into two groups of bands, the lowest one consisting of three components and the highest one of two components, as in the case of an octahedral type crystal field with a  $T_2$  state at lower energy than a E state.

Although many details must be deferred to a future work, a little more can be said to understand the complexity of the problem to be solved. Considering first the energy levels of the 4f5d electronic configuration for the free ion, as reported in Ref. 27, the energy spacings (a few thousands  $\text{cm}^{-1}$ ) between the different spectral terms resulting from the 4f-5d electrostatic interaction have comparable magnitude to that produced by the local crystal field on the 5d orbitals. Consequently, it is likely that the electrostatic and local distortion hamiltonians should have to be treated together. At the moment, we can only predict the nature and the symmetry of the resulting states without knowing their respective energies.

Let us consider the case of  $\text{Pr:LiYF}_4$  for which complete ground state absorption data are available [9]. The local site symmetry is  $S_4$ , so that the 5d(e) orbital component of lower energy (in  $T_d$  symmetry), state  $5d(^2E)$ , splits into two spin-doublets  $^2\Gamma_1$  and  $^2\Gamma_2$  (with Bethe notation [see in Ref. 28 for definitions]). On the other hand, neglecting spin-orbit interaction with respect to electrostatic interaction, the orbital wave functions of the 4f electron, i.e. of the  $4f(^2F)$  state, transform like (using the decomposition of the reducible representation  $D_3$  for  $l = 3$ )  $\Gamma_1 + 2\Gamma_2 + 2\Gamma_{3,4}$  (or  $A + 2B + 2E$  using Mulliken notation). So, electrostatic coupling  $4f(^2F)5d(^2E)$  should result in two sets of spin-singlets and spin-triplets which we can label  $^{1,3}\Gamma_{E1}$  and  $^{1,3}\Gamma_{E2}$  with :

$$\begin{aligned} \Gamma_{E1} &= \Gamma_1 \times (\Gamma_1 + 2\Gamma_2 + 2\Gamma_{3,4}) = \Gamma_1 + 2\Gamma_2 + 2\Gamma_{3,4} \\ \text{and} \quad \Gamma_{E2} &= \Gamma_2 \times (\Gamma_1 + 2\Gamma_2 + 2\Gamma_{3,4}) = \Gamma_2 + 2\Gamma_1 + 2\Gamma_{3,4} \end{aligned}$$

Then, the same decompositions can be done for the  $^3H_4$  ground state and the  $^3P_0$  and  $^1D_2$  excited states. With the electric dipole selection rules for the different crystal symmetries, attempts can then be made to propose some order in the 4f5d energy levels, but it is preferable to wait for more data (low temperature data and spectra recorded over a more extended wavelength domain) and specific calculations to do so. It is interesting to note, however, that the ground state absorption spectra alone certainly cannot reveal all the 4f5d energy levels and that many different energy levels can be reached via ESA transitions, as we have actually observed.

#### 4. Excited state excitation and two-step pumping model :

The different ESA spectra reported above confirm that two-step excitation should be an efficient up-conversion process to populate 4f5d energy levels in Pr doped fluoride and oxide perovskite crystals. Compared to other excited-state absorptions between energy levels all resulting from the same  $4f^n$  configuration, which is the usual case encountered for upconversion in RE doped laser materials, the second step is here greatly enhanced because of the high value of the  $4f^2 \rightarrow 4f5d$  ESA cross sections ( $\sigma_{ESA}$  is three orders of magnitude higher than for intraconfigurational ESA transitions). Even if the excited-state ion density obtained after the first pumping step is limited to only a few percent of the dopant concentration, the second step can efficiently bleach the intermediate metastable level and gives rise to a final 4f5d population with significant density compared to a direct  $4f^2 \rightarrow 4f5d$  excitation.

To demonstrate such a two-photon effect experimentally, we simultaneously sent first onto our Pr :LiYF<sub>4</sub> sample the signal wave of the OPO at about  $\lambda_1 = 450$  nm and part of the pump residue at  $\lambda_2 (^3P_0 \rightarrow 4f5d) = 355$  nm (third harmonic of the Nd:YAG laser). According to Fig. 11, the ESA cross section at  $\bar{\nu}(4f5d) = \bar{\nu}(^3P_0) + \bar{\nu}(^3P_0 \rightarrow 4f5d) = 49030 \text{ cm}^{-1}$  (with a value of about  $0.4 \times 10^{-18} \text{ cm}^2$  in  $\sigma$  polarization) is far from being maximum but the use of the pump residue has the advantage of facilitating the temporal and the spatial overlap of the two pulsed pump beams. A schematic representation of the two-step pumping process can be found in Fig. 8. As expected, though the second pump source is not perfectly adequate, the stepwise excitation gives rise to a strong UV emission and the registered fluorescence spectrum is exactly the same as the one reported in Fig. 6.

Similar results were obtained in the case of Pr : KY<sub>3</sub>F<sub>10</sub> and Pr : BaY<sub>2</sub>F<sub>8</sub>.

We investigated further the efficiency of this two-step pumping process by estimating the single pass gain which can be obtained from such a potential UV laser system. We assumed two pulsed laser beams with  $\tau_{p1} = \tau_{p2} = 5$  ns time duration and energies  $E_1 = E_2 = 1$  mJ each and focused on cross sections  $s_1 = s_2 = 2 \times 10^{-3}$  cm<sup>2</sup> of a sample of length  $l = 2$  mm (which means pump fluences of 0.5 J/cm<sup>2</sup>, which is generally enough, for example, to reach laser threshold with Ce doped laser crystals [see in Refs 20 and 29 for example]). With a system such as Pr : KY<sub>3</sub>F<sub>10</sub>, the first excitation step is realized with a laser tuned at  $\lambda_1 = 445$  nm ( $^3H_4 \rightarrow ^3P_2$  GSA cross section  $\sigma_1 = 3.75 \times 10^{-20}$  cm<sup>2</sup>) and the second one at  $\lambda_2 = 355$  nm ( $^3P_0 \rightarrow 4f5d$  ESA cross section  $\sigma_2 = 0.4 \times 10^{-18}$  cm<sup>2</sup>). Denoting  $N_1$ ,  $N_2$  and  $N_3$  the instantaneous populations of the  $^3H_4$  ground state, the  $^3P_{0,1,2}$  excited multiplet and the 4f5d electronic configuration, respectively, the single pass gain, given by

$$G = \exp[(N_3 \sigma_{SE}(\lambda_g) - N_2 \sigma_{ESA}(\lambda_g))l] \quad (7)$$

can be calculated by solving the following system of rate equations.

$$\begin{aligned} \frac{\partial N_1}{\partial t} &= \frac{N_2}{\tau_2} \beta_{21} + \frac{N_3}{\tau_3} \beta_{31} - \frac{E_1 \sigma_1 \lambda_1}{\tau_{p1} h c s_1} f_1(t) N_1 \\ \frac{\partial N_2}{\partial t} &= -\frac{N_2}{\tau_2} + \frac{E_1 \sigma_1 \lambda_1}{\tau_{p1} h c s_1} f_1(t) N_1 - \frac{E_2 \sigma_2 \lambda_2}{\tau_{p2} h c s_2} f_2(t) N_2 \\ \frac{\partial N_3}{\partial t} &= -\frac{N_3}{\tau_3} + \frac{E_2 \sigma_2 \lambda_2}{\tau_{p2} h c s_2} f_2(t) N_2 \end{aligned} \quad (8)$$

Here, the branching ratios for the  $^3P_0$  and 4f5d emissions down to the ground state  $\beta_{21}$  and  $\beta_{31}$  are set equal to 1. Their respective fluorescence lifetimes are given by  $\tau_2 = 30$   $\mu$ s and  $\tau_3 = 26$  ns and  $f_1$  and  $f_2$  stand for the normalized gaussian shapes of the pump pulses.  $\sigma_{SE} = 1.2 \times 10^{-18}$  cm<sup>2</sup> and  $\sigma_{ESA} = 0.05 \times 10^{-18}$  cm<sup>2</sup> are the cross sections of the 4f5d stimulated emission and of the  $^3P_0 \rightarrow 4f5d$  ESA transition at the choosen probe emission wavelength  $\lambda_g = 266$  nm.

The result of this simulation is reported in Fig. 17. The second pump pulse was intentionally delayed from the former by about 6 ns and, in these conditions, gain reaches a maximum some 17 ns later with a value  $G = 1.2$ , which means 20% gain per pass. It is worth remembering, however, that this

simulation is made by assuming negligible ESA of the pump and emitted photons in the 4f5d emitting state, which might be the case at particular wavelengths and/or for particular polarization conditions but which has not yet been proven.

#### 5. Tentative gain measurements:

Measurements of UV laser gain were attempted in all the materials at a wavelength of 266 nm and by pumping them, as shown in the Figure 18, with two consecutive photons at 470 nm (to excite the  $^3P_{0,1,2}, ^1I_6$  multiplets) and 355 nm (to reach the 4f5d band from the  $^3P_{0,1,2}, ^1I_6$  excited multiplet). Gain was attempted at 266 nm first because it was the only probe wavelength which was not too difficult to produce with our Nd:YAG pumped OPO laser (by frequency doubling the residual of the 532 nm radiation), second, because this probe was at a longer wavelength than that already tried unsuccessfully [12] around 225 nm in Pr:LiYF<sub>4</sub> and Pr:BaY<sub>2</sub>F<sub>8</sub> (but also in Pr:CaF<sub>2</sub> and several other similar fluorides). Unfortunately, this probe wavelength either probably correspond to too weak emission cross sections - it is the case of Pr:LiYF<sub>4</sub> or Pr:BaY<sub>2</sub>F<sub>10</sub> (see in Fig. 6) - this wavelength was perfectly adapted - it is the case of Pr:KY<sub>3</sub>F<sub>10</sub> or Pr:YAlO<sub>3</sub> (see in Figs 5 and 6) - but the crystals solarised so much that it was impossible to detect any laser gain.

#### 6. Solarisation experiments:

As mentioned in the beginning, solarisation, i.e. creation of color centers under UV light excitation, is a critical problem in most of these UV emitting materials. However, it has been demonstrated, at least in the case of the now famous Ce:LiCAF and Ce:LiSAF laser systems that these solarisation effects not only depend on the characteristics of the optical transitions such as polarization but also on the purity and the dopant substitution process of the crystals. Concerning the first aspect, solarisation was attributed to ESA (of the pump and/or the emitted photons from the 5d UV emitting state up into the conduction band of the crystals) followed by trapping of the resulting free electrons by impurity traps (traps resulting by incomplete charge compensation in the doping process, in the case of Ce:LiCAF and Ce:LiSAF). We have not tried yet to pump directly our Pr doped crystals into their 4f5d band to check this problem because the 213 nm Nd:YAG laser pump source necessary for that was not available. However, we could observe some solarisation effects in the course of the two-photon excitation experiments that we

described in section 4, as well as during our tentative gain measurements discussed in section 5. These solarisation effects manifested themselves by the appearance of broad absorption bands in the blue/UV domain (see in Figs 19 and 20), extending, for example, from 240 to 320 nm and from 350 to 550 nm in the case of Pr:KY<sub>3</sub>F<sub>10</sub> (see in Fig. 19) and from 250 to 650 nm in the case of Pr:YAlO<sub>3</sub> (see in Fig. 20). Concerning these last two systems, it is worth noting the two following points. Solarisation effects in Pr:KY<sub>3</sub>F<sub>10</sub> strongly depend on crystal quality and in the case of Pr:YAlO<sub>3</sub>, it seems that solarisation effects are decreasing as the dopant concentration is increased. In the case of Pr:KY<sub>3</sub>F<sub>10</sub>, a poor optical quality also means a larger number of lattice defects, so a larger number of potential trap centers for the free electrons produced in the conduction band. In the case of Pr:YAlO<sub>3</sub>, solarisation effects could be reduced very significantly by increasing the Pr dopant concentration. This is in agreement with a previous work [31] in which it was shown that the color centre formation in YAlO<sub>3</sub> mainly comes from the formation of electron-hole pairs followed by trapping of holes by Pr<sup>3+</sup> ions, thus by the formation of Pr<sup>4+</sup> (Pr<sup>3+</sup> + e<sup>+</sup> → Pr<sup>4+</sup>). However, the reverse electron capture process at Pr<sup>4+</sup> ions also occurs (Pr<sup>4+</sup> + e<sup>-</sup> → Pr<sup>3+</sup>). So, Pr<sup>3+</sup> ions, serving as additional traps, change the direction of processes of charge carriers release and capture which results in an increase of the material stability to short wavelength radiation.

These results both mean that better quality crystals need to be grown and that dopant concentration can be a very important parameter.

## CONCLUSIONS and RECOMMENDATIONS

This work reports for the first time detailed  $4f^n-4f^{n-1}5d$  interconfigurational ESA spectra for a trivalent rare earth ion, here  $\text{Pr}^{3+}$  ( $n=2$ ), in various selected fluoride crystals,  $\text{KY}_3\text{F}_{10}$ ,  $\text{LiYF}_4$  and  $\text{BaY}_2\text{F}_8$  and  $\text{KYF}_4$  and an oxide,  $\text{YAlO}_3$ . These Pr doped crystals were selected among many others for several reasons. They were selected first for their emission properties in the near UV spectral domain and their potential use as amplifier media in tunable UV laser systems. They were also selected because most of them can be grown in large enough dimensions by using conventional techniques such as the Bridgman or the Czochralski techniques, but also because we had the possibility to grow the fluorides in our own laboratory and we had the possibility to get the oxide via existing collaborations with foreign specialists. Finally, we gave our preference to the  $\text{Pr}^{3+}$  ion both because of fundamental and practical reasons. Indeed,  $\text{Pr}^{3+}$  is the ion coming right after the  $\text{Ce}^{3+}$  lasing ion in the lanthanide series so that a lot of information coming from the spectroscopic and laser properties of the latter can be used to understand and predict the properties of the former. From the application point of view,  $\text{Pr}^{3+}$  ion was also chosen because it gives access to a shorter wavelength, thus complementary, emission domain than  $\text{Ce}^{3+}$ , and most importantly, its broad band UV emission can be pumped sequentially by using a two-step excitation scheme, the involved blue/near-UV pump photons being less detrimental for the materials (less solarisation effects).

From the spectroscopic point of view, the complex electronic structure of the first excited electronic configuration  $4f5d$  for  $\text{Pr}^{3+}$  (the one giving rise to UV emission) has been clearly demonstrated. Because they are both polarized and better spectrally resolved, ESA spectra reveal much more structures than unpolarized ground state absorption or excitation spectra performed in the VUV domain. Though ESA spectra associated with the absorbing spin singlet and spin triplet  $^1D_2$  and  $^3P_0$ , respectively, differ significantly with the appearance of distinct energy levels, it is hard to say at the moment whether this distinction is linked with any spin or angular momentum selection rule, as in the case of a pure L-S coupling. A definitive assignment will have to await low temperature data and specific calculations considering crystal field and electrostatic interactions altogether.

These ESA measurements have permitted us to predict an optimized wavelength for the second step under two-photon excitation using a step-by-step mechanism. This upconversion process is a possible way to alleviate the solarization problems and also to overcome the lack of practical pump sources in the near UV. **The simulation of such upconversion pumping reported in this study is thus encouraging.** Assuming negligible ESA in the emitting level, which is probably too optimistic, 20% laser gain per pass is demonstrated. Gain measurements using synchronized pump laser radiations and a probe beam which can be tuned to the various emission peaks are underway.

From the **prospective** point of view, we also have conducted a comparative study of all the ground- and excited-state absorption and emission properties of the presently known materials doped with  $\text{Ce}^{3+}$  ( $4f \leftrightarrow 5d$  transitions),  $\text{Pr}^{3+}$  ( $4f^2 \leftrightarrow 4f5d$ ) and  $\text{Nd}^{3+}$  ( $4f^3 \leftrightarrow 4f^25d$ ), taking into account the positions of the energy levels of these active ions within the bandgap of the host matrices. The situation can be presented, with the three energy level diagrams reported in the Figures 19 and 20, as follows:

- $\text{Ce}^{3+}$  doped LiCAF and LiSAF lased because ESA in the emission domain (285-315 nm) of these materials hardly reach their conduction band. It means that some solarisation effects - inherent to the problem of charge compensation mentioned in section 6 - can occur but that they can be significantly limited by **addressing the crystal growth question before all.** This assertion is confirmed with the case of  $\text{Ce}^{3+}$  in  $\text{LiYF}_4$  and  $\text{LiLuF}_4$  since no charge compensation is needed to incorporate the dopant ion in these materials and so, provided they are good quality crystals, solarisation effects should be very much reduced; this is indeed what we observed in the course of a parallel study of these Ce doped materials since no solarisation effect could be observed in  $\text{Ce:LiLuF}_4$  and only weak effects could be observed in  $\text{Ce:LiYF}_4$  by pumping the crystals with an excimer laser at 248 nm up to  $4\text{J}/\text{cm}^2$  (which is much higher than the laser threshold pump fluence [29]).

- the case of the  $\text{Pr}^{3+}$  doped fluoride crystals, in general, and of the  $\text{Pr}^{3+}$  doped oxides such as the one more particularly studied in this work ( $\text{YAlO}_3$ ) is more critical. Indeed, it seems that there is no possibility to avoid ESA of the emitted photons into the conduction band of the materials, except for the longer wavelength emitted photons. Consequently, it would be worth studying  $\text{Pr}^{3+}$  doped materials with emissions at longer wavelengths, while characterized by reduced Stokes shifts (since a large Stokes shift is detrimental for the fluorescence quantum efficiency) and by large energy gaps. **Two**

kinds of crystals meet these two requirements and are worth to be investigated in a future work: Pr:elpasolites [32] such as  $\text{Cs}_2\text{NaYF}_6$  [33] and Pr:borates such as  $\text{XBO}_3$  with  $X = Y, \text{Sc}, \text{Lu}$  [34] with emissions between 260 and 310 nm.

- the  $\text{Nd}^{3+}$  doped fluorides (and other materials characterized by large energy gaps), assuming the previous statements (concerning the importance of the energy level positions within the bandgap) are correct, might offer very interesting possibilities. Indeed, in this case, ESA transitions of the emitted photons might end above the conduction band of the host material. This is probably what happens in the case of  $\text{Nd}:\text{LaF}_3$ , a system which already lased in the past at 172 nm when pumped by a  $\text{F}_2$  molecular laser at 157 nm [34]. So, it can be very interesting to reexamine these  $\text{Nd}^{3+}$  doped fluorides, but now by considering a two- or a three- step excitation pumping scheme involving visible/blue instead of UV photons (as in the case of  $\text{Pr}^{3+}$ ).

### Literature cited:

1. A. Bleckman, F. Heine, J.P. Meyn, T. Danger, E. Heumann and G. Huber, OSA Proceedings on Advanced Solid State Lasers, A.A. Pinto and T.Y. Fan eds., (Optical Society of America, Washington, DC, 1993), vol. 15, pp. 199-201.
2. L.D. Deloach et al, in OSA Proceed. on Advanced Solid State Lasers, A.A. Pinto and T.Y. Fan, eds (Optical Society of America, Washington DC 1993) vol. 15 pp 188-191
3. G. Blasse et al, J. Phys. Chem. Sol. 50 (1989) 583
4. M. Malinowski, C. Garapon, M. F. Joubert and B. Jacquier, J. Phys. Condens. Matter 7 (1995) 199
5. E. G. Gumanskaya, M. V. Korzhik, S.A. Smirnova, V.B. Pavienko and A.A. Fedorov, Opt. Spectrosc. 72 (1991) 86
6. C. Pédrini, D. Bouttet, C. Dujardin, B. Moine, I. Dafinei, P. Lecoq, M. Koselja and K. Blazek, Opt. Mat. 3 (1994) 81.
7. T. Tomiki, F. Kaminao, M. Fujisawa and Y. Tanahara, J. Phys. soc. Japan 55 (1986) 2090.
8. T. Tomiki, F. Kaminao, M. Fujisawa, Y. Tanahara and T. Fudemna, J. Lumin. 40&41 (1988) 379.
9. L. Esterowitz, F.J. Bartoli, R.E. Allen, D.E. Wortman, C.A. Morrison, R.P. Leavitt, « Energy levels and line intensities of  $\text{Pr}^{3+}$  in  $\text{LiYF}_4$  », Phys. Rev. B 19 (1979) 6442-6455
10. G.M. Renfro, J.C. Windscheif, W.A. Sibley, R.F. Belt, « optical transitions of  $\text{Pr}^{3+}$  and  $\text{Er}^{3+}$  ions in  $\text{LiYF}_4$  », J. Lumin. 22 (1980) 51-68
11. J.L. Adam, W.A. Sibley, D.R. Gabbe, « Optical absorption and emission of  $\text{LiYF}_4:\text{Pr}^{3+}$  », J. Lumin. 33 (1985) 391-407
12. J.K. Lawson, S.A. Payne, « Excited-state absorption of  $\text{Pr}^{3+}$ -doped fluoride crystals », Opt. Mat. 2 (1993) 225-232
13. W.W. Piper, J.A. DeLuca, F.S. Ham, « Cascade fluorescence decay in  $\text{Pr}^{3+}$ -doped fluorides : achievement of a quantum yield greater than unity for emission of visible light », J. Lumin. 8 (1974) 344-348
14. B.M. Antipenko, « Spectroscopic properties of the system  $\text{BaYb}_2\text{F}_8$  :rare earth ions », Opt. Spektrosc. 56 (1984) 72-77
15. A.A. Kaminskii, S.E. Sarkisov, « Stimulated-emission spectroscopy of  $\text{Pr}^{3+}$  ions in monoclinic  $\text{BaY}_2\text{F}_8$  fluoride », Phys. Stat. Sol. (a) 97 (1986) K163-K168
16. S.P. Chernov, L.I. Devyatkov, O.N. Ivanova, A.A. Kaminskii, V.V. Mikhailin, S.N. Rudnev, T.V. Uvarova, «  $5d^{14}f^{n-1}-4f^n$  absorption and luminescence of  $\text{Ce}^{3+}$ ,  $\text{Pr}^{3+}$  and  $\text{Nd}^{3+}$  ions in  $\text{BaY}_2\text{F}_8$  single crystals », Phys. Stat. Sol. (a) 88 (1985) K169-K173
17. C.A. Morrison, D.F. Wortman, R.P. Leavitt, H.P. Jenssen, « Assessment of  $\text{Pr}^{3+}:\text{KY}_3\text{F}_{10}$  as blue-green laser », Harry Diamond Labs report (USA) HDL-TR 1897 (1980)

18. R.A. MacFarlane, « Upconversion laser in  $\text{BaY}_2\text{F}_8:\text{Er}$  5% pumped by ground-state and excited-state absorption », J. Opt. Soc. Am. B 5 (1994) 871-880
19. R. Diehl, G. Brandt ; Mat. Res. Bull. 10 (1975) 85
20. C.D. Marshall, S.A. Payne, J.E. Speth, W.F. Krupke, G.J. Quarles, V. Castillo, B.H.T. Chai, "Ultraviolet laser emission properties of  $\text{Ce}^{3+}$  doped  $\text{LiSrAlF}_6$  and  $\text{LiCaAlF}_6$ ", J. Opt. Soc. Am. B 11 (1994) 2054-2065; A.J. Bayramian, C.D. Marshall, S.A. Payne et al; Advanced Solid State Lasers (San Francisco 96)
21. S. Zhang, J. Lumin. 40-41 (1988) 159
22. K.H. Yang, J.A. Deluca « Vacuum-ultraviolet excitation studies of  $5d^1 4f^{n-1}$  to  $4f^n$  and  $4f^n$  to  $4f^n$  transitions of  $\text{Nd}^{3+}$ -,  $\text{Er}^{3+}$ - and  $\text{Tm}^{3+}$ - doped trifluorides », Phys. Rev. B 17 (1978) 4246-4255
23. J.C. Krupa, M. Queffelec, « UV and VUV optical excitations in wide band gap materials doped with rare earth ions :  $4f$ - $5d$  transitions », J. Alloys Comp. 250 (1997) 287-292
24. E. Sarantopoulou, A.C. Cefalas, M.A. Dubinskii, C.A. Nicolaides, R.Yu. Abdulsabirov, S.L. Korableva, A.K. Naumov, V.V. Semasko, « VUV and UV fluorescence and absorption studies of  $\text{Pr}^{3+}$ -doped  $\text{LiLuF}_4$  single crystals », Opt. Lett. 19 (1994) 499-501
25. A.A. Kaplyanski, A.K. Przhhevuskii, « Deformation splitting and enhancement of spectral lines and structure of excited levels of  $\text{Eu}^{2+}$  in alkali-earth fluoride crystals », Opt. Spectrosc. 19 (1965) 331-338
26. T. Hoshina, S.Z. Kuboniwa, «  $4f$ - $5d$  transition of  $\text{Tb}^{3+}$  and  $\text{Ce}^{3+}$  in  $\text{MPO}_4$  ( $\text{M}=\text{Sc}$ ,  $\text{Y}$  and  $\text{Lu}$ ) », J. Phys. Soc. Jap. 31 (1971) 828-840
27. J. Sugar, « Analysis of the spectrum of triply ionized Praseodymium ( $\text{PrIV}$ ) », J. Opt. Soc. Am. 55 (1965) 1058-1061
28. J.S. Griffith ; « The theory of transition-metal ions », Cambridge University Press 1964
29. P. Rambaldi, R. Moncorgé, J.P. Wolf, C. Pedrini, J.Y. Gesland, « Efficient and stable pulsed laser operation of  $\text{Ce}:\text{LiLuF}_4$  around 308nm », OSA TOPS vol. 19, Advanced Solid State Lasers, W.R. Bosenberg, M.Fejer (eds), p10; Opt. Comm. 146 (1998) 163-166
30. M.J. Weber, J. Appl. Phys. 44 (1973) 3206
31. T.I. Butaeva, K.L. Ovanesyan and A.G. Petrosyan; Cryst. Res. Tech. 23 (1988) 849
32. M. Laroche et al (to be published in Chem. Phys. Lett.)
33. B.F. Aull, H.P. Jenssen, Phys. Rev. B34 (1986) 6647
34. G. Blasse, J.P.M. Van Vliet, J.W.M. Verwey, R. Hoogendam, M. Wiegel; J. Phys. Chem. Sol. 50 (1989) 583
35. R.W. Waynant, P.H. Klein; Appl. Phys. Lett. 46 (1985) 14

## Figure Captions :

- Fig.1: Ground-state absorption of  $\text{Pr:YAlO}_3$  in the visible domain
- Fig.2: Ground-state absorption of  $\text{Pr:YLiF}_4$  and  $\text{Pr:KY}_3\text{F}_{10}$  in the visible domain
- Fig.3: Ground-state absorption of  $\text{Pr:BaY}_2\text{F}_8$  in the visible domain
- Fig.4: Ground-state absorption of  $\text{Pr:KYF}_4$  in the visible domain
- Fig.5: Unpolarized UV emission spectra of  $\text{Pr:YAlO}_3$
- Fig.6: Unpolarized UV emission spectra of  $\text{Pr:KY}_3\text{F}_{10}$ ,  $\text{Pr:YLiF}_4$  and  $\text{Pr:BaY}_2\text{F}_8$
- Fig.7: Unpolarized UV emission spectra of  $\text{Pr:KYF}_4$
- Fig.8: Energy level scheme for  $\text{Pr}^{3+}$  in  $\text{LiYF}_4$
- Fig.9: ESA experimental set-up
- Fig.10: Excited-state absorption spectra of  $\text{Pr:KY}_3\text{F}_{10}$  from the  $^1\text{D}_2$  and  $^3\text{P}_{0,1,2}+^1\text{I}_6$  multiplets
- Fig.11: Polarized excited-state absorption spectra of  $\text{Pr:YLiF}_4$  from the  $^1\text{D}_2$  and  $^3\text{P}_{0,1,2}+^1\text{I}_6$  multiplets
- Fig.12: Polarized excited-state absorption spectra of  $\text{Pr:Pr:BaY}_2\text{F}_8$  from the  $^1\text{D}_2$  and  $^3\text{P}_{0,1,2}+^1\text{I}_6$  multiplets
- Fig.13: Polarized excited-state absorption spectra of  $\text{Pr:YAlO}_3$  from the  $^1\text{D}_2$  and  $^3\text{P}_{0,1,2}+^1\text{I}_6$  multiplets
- Fig.14: Polarized excited-state absorption spectra of  $\text{Pr:KYF}_4$  from the  $^3\text{P}_{0,1,2}+^1\text{I}_6$  multiplet
- Fig.15: 4f5d energy levels according to the  $^3\text{H}_4 \rightarrow 4\text{f}5\text{d}$  and the  $^3\text{P}_0 \rightarrow 4\text{f}5\text{d}$  and  $^1\text{D}_2 \rightarrow 4\text{f}5\text{d}$  ESA spectra of  $\text{Pr:KY}_3\text{F}_{10}$ ,  $\text{Pr:LiYF}_4$  and  $\text{Pr:BaY}_2\text{F}_8$
- Fig.16: 4f5d energy levels according to the  $^3\text{H}_4 \rightarrow 4\text{f}5\text{d}$  and the  $^3\text{P}_0 \rightarrow 4\text{f}5\text{d}$  and  $^1\text{D}_2 \rightarrow 4\text{f}5\text{d}$  ESA spectra of  $\text{Pr:YAlO}_3$
- Fig.17: Temporal evolutions of the  $^3\text{H}_4$  ground state,  $^3\text{P}_{0,1,2}$  excited multiplet and 4f5d electronic configuration populations  $N_1$ ,  $N_2$  and  $N_3$  after two-step excitation pumping
- Fig.18: Experimental set-up used for measurements of laser gain at 266 nm and solarisation spectra after two-step excitation with 470 and 355 nm pump photons
- Fig.19: Solarisation absorption spectrum observed in  $\text{Pr:KY}_3\text{F}_{10}$  after two-step excitation pumping at 470 and 355 nm
- Fig.20: Solarisation absorption spectrum observed in  $\text{Pr:YAlO}_3$  after two-step excitation pumping at 470 and 355 nm
- Fig.21: Relative positions of the  $\text{Pr}^{3+}$  energy levels and of the valence and conduction bands in various materials
- Fig.22: Relative positions of the  $\text{Pr}^{3+}$  energy levels and of the valence and conduction bands in various materials
- Fig.23: Relative positions of the  $\text{Pr}^{3+}$  and  $\text{Nd}^{3+}$  energy levels and of the valence and conduction bands in various materials

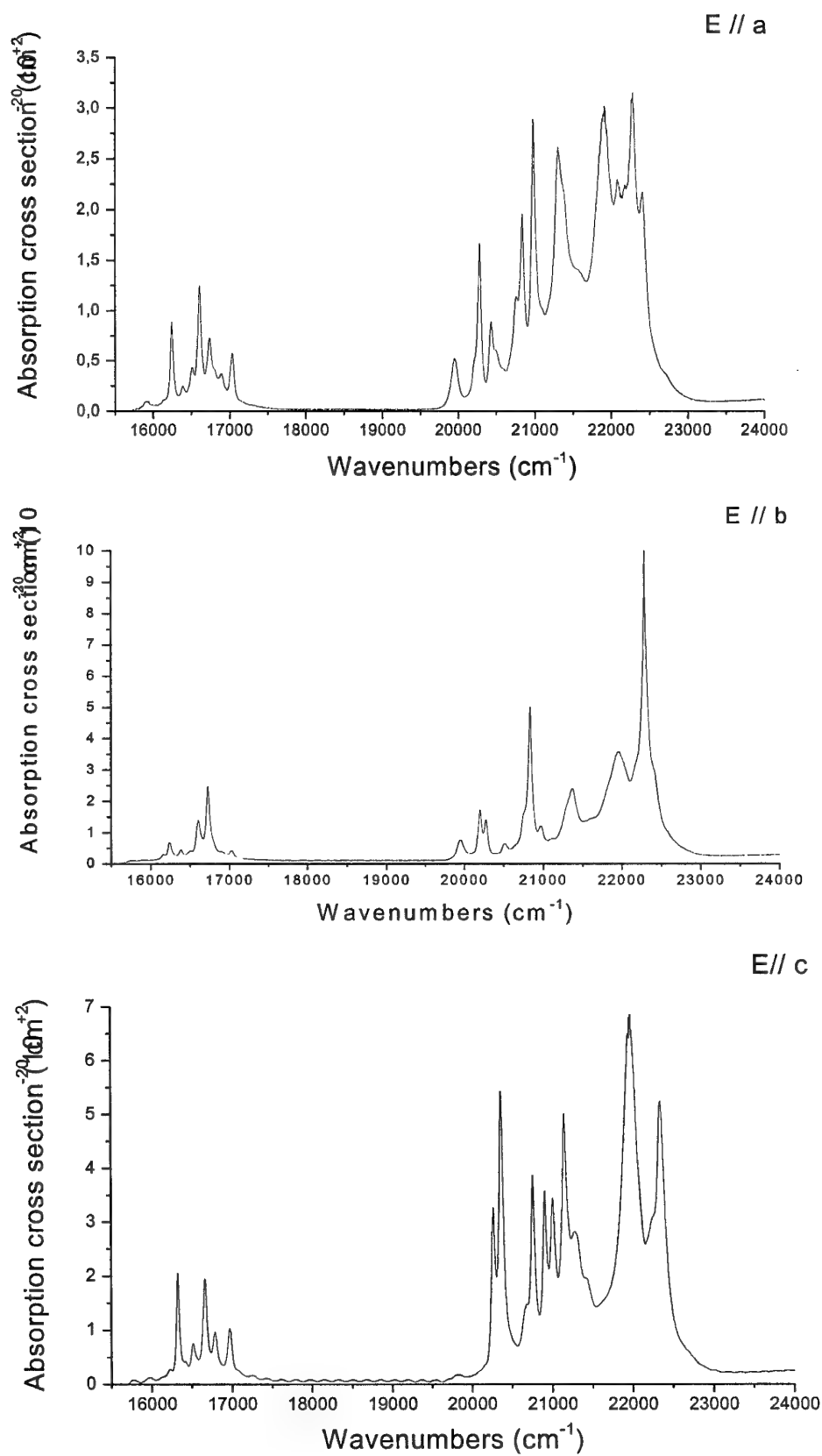


Fig 1: Polarized ground state absorption spectra of  $\text{Pr:YAlO}_3$

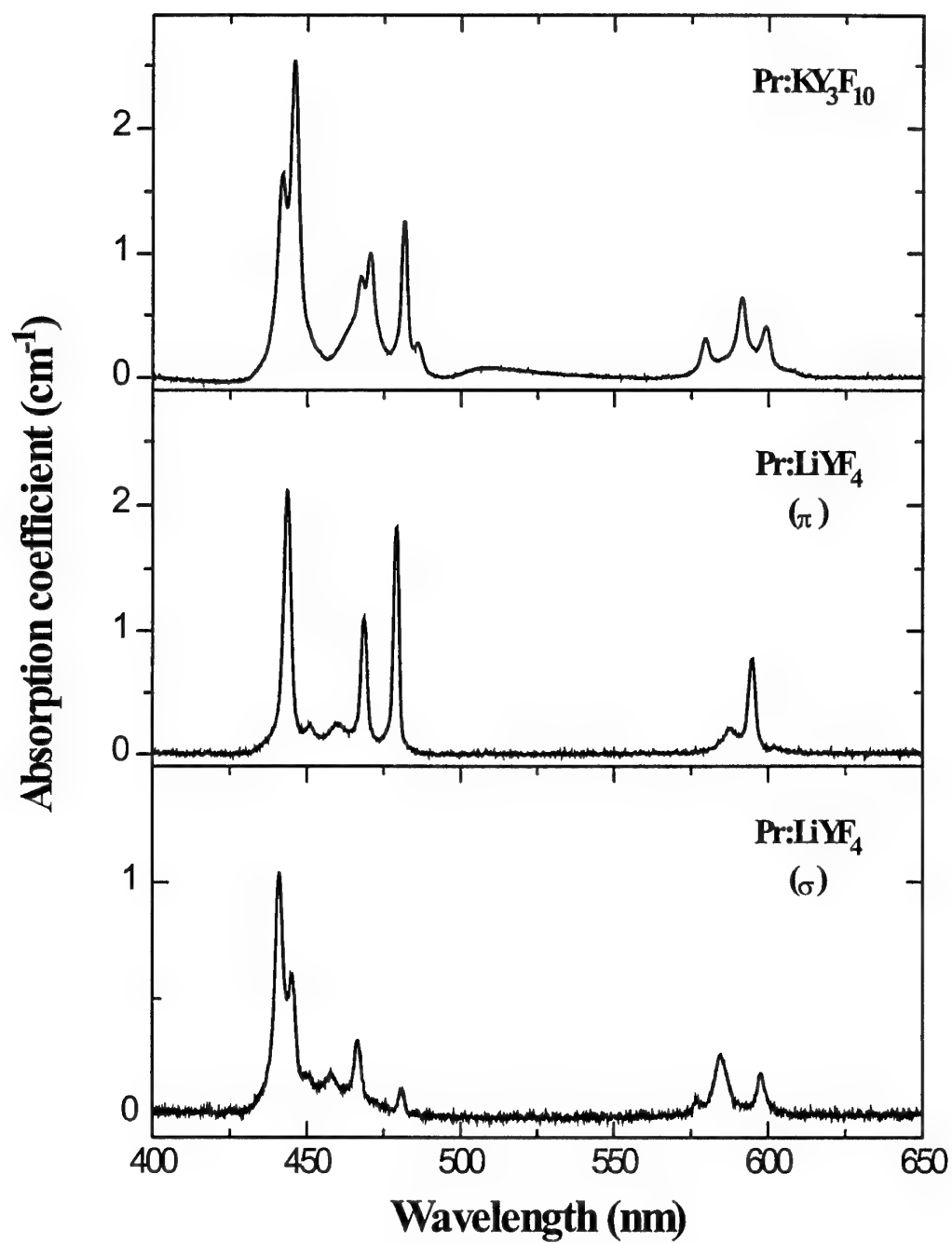


Fig. 2: Ground-state absorption of Pr:YLiF<sub>4</sub> and Pr:KY<sub>3</sub>F<sub>10</sub> in the visible domain

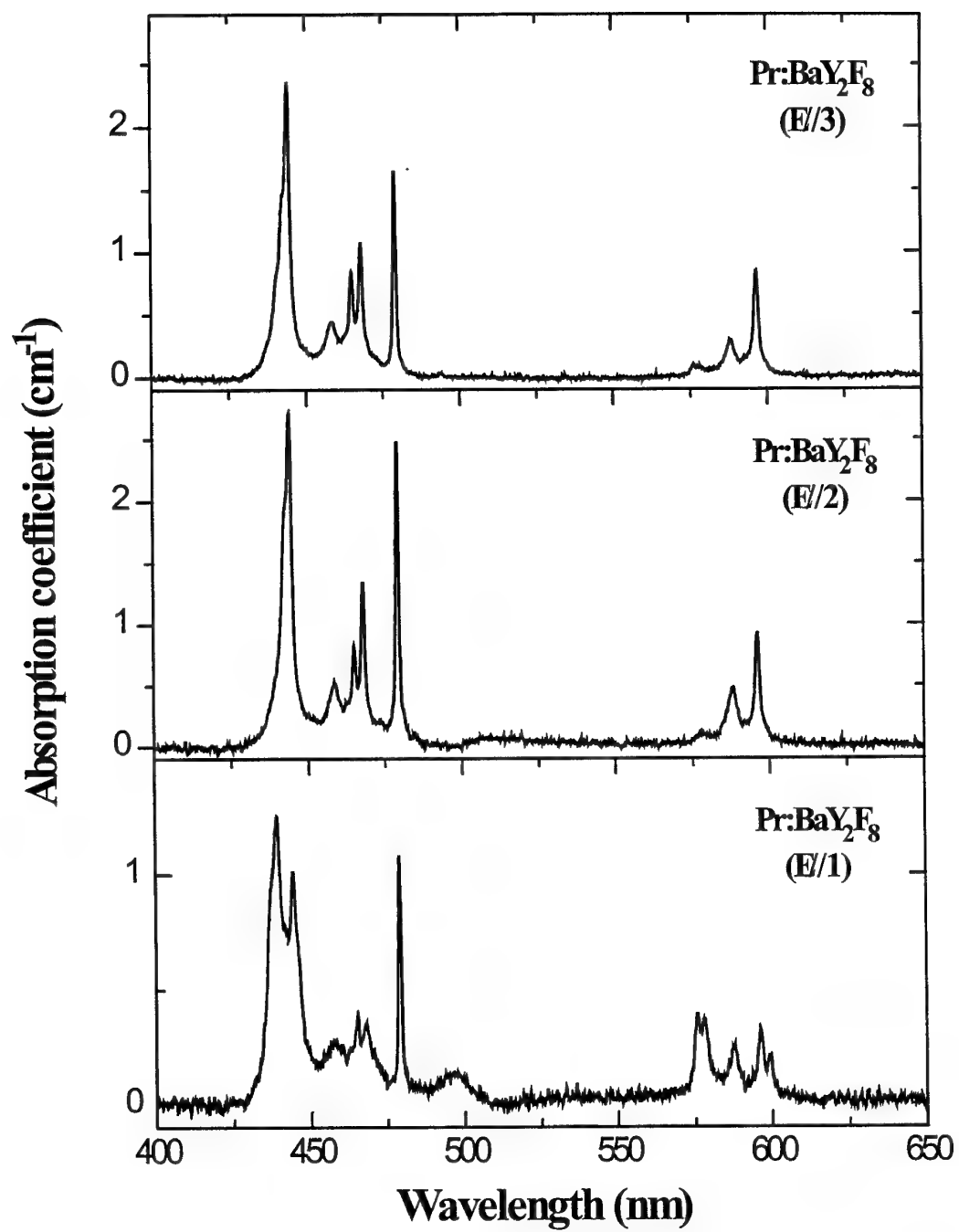


Fig. 3: Ground-state absorption of  $\text{Pr:BaY}_2\text{F}_8$  in the visible domain

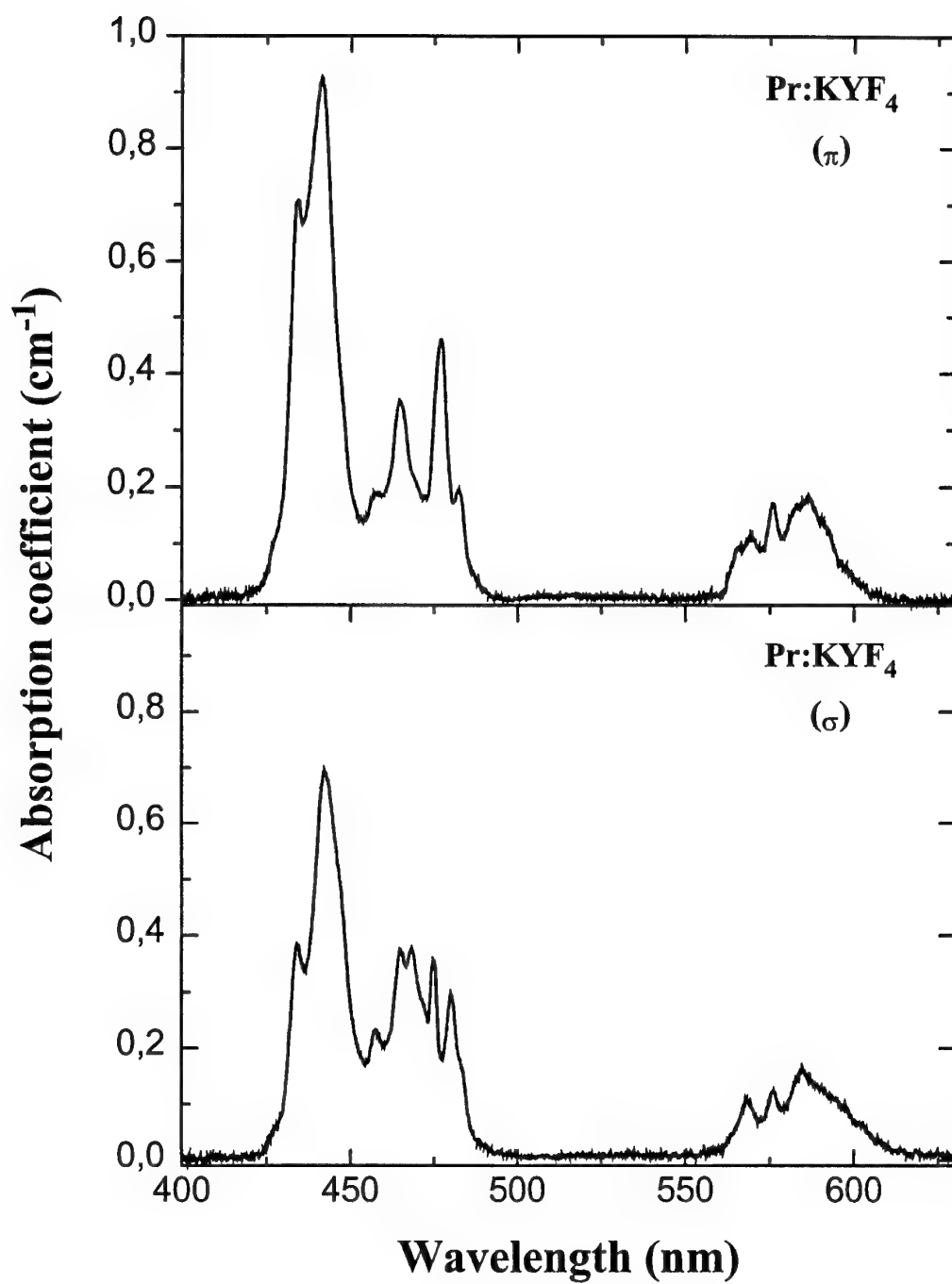


Fig. 4: Ground-state absorption of Pr:KYF<sub>4</sub> in the visible domain

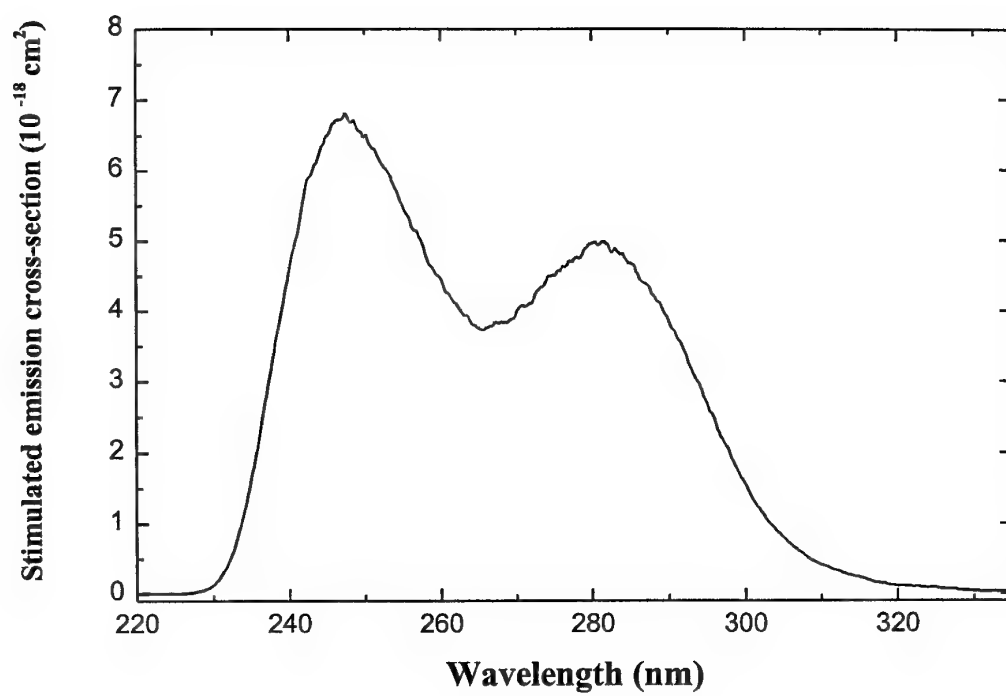


Fig. 5: Unpolarized emission spectra of Pr:YAlO<sub>3</sub>

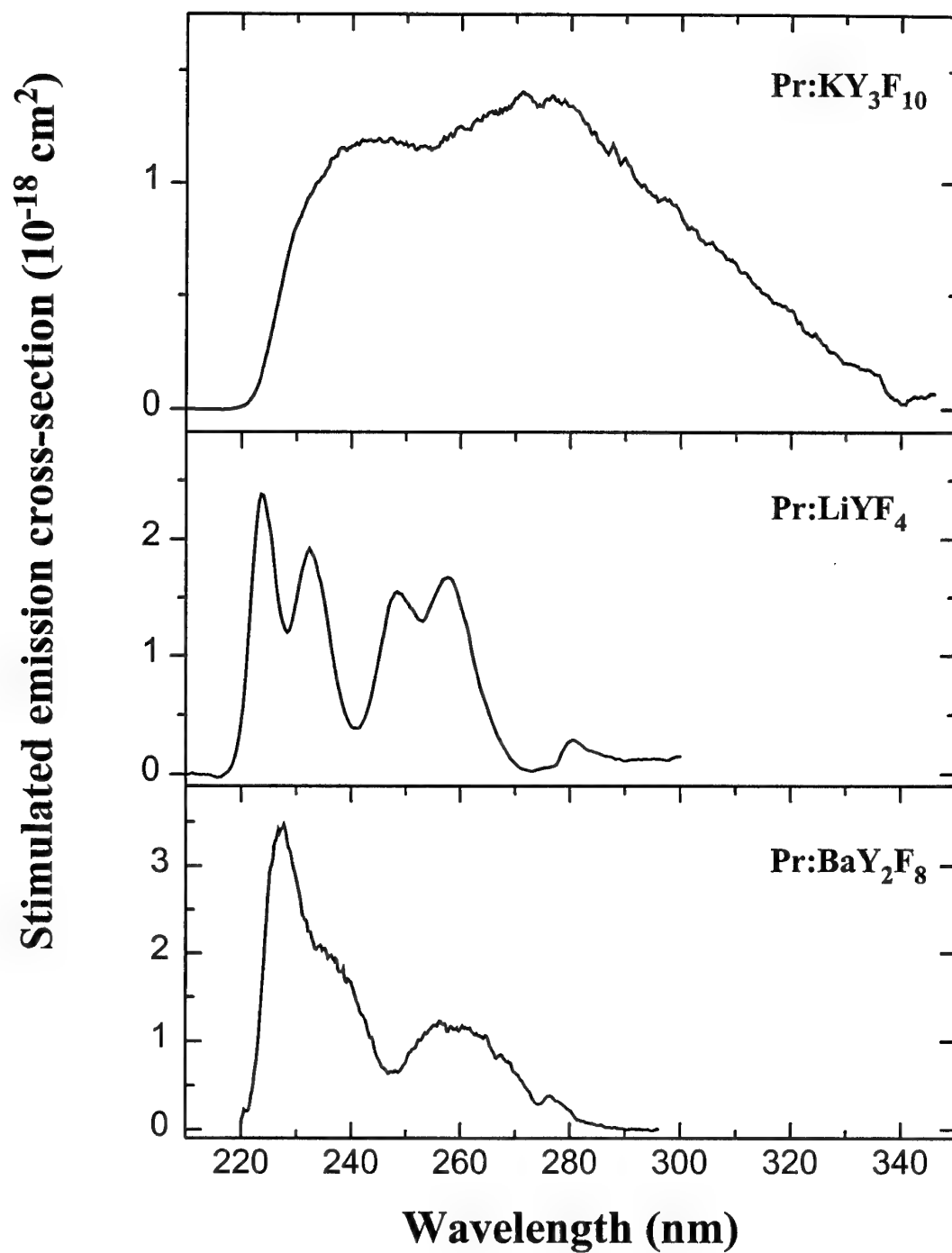


Fig. 6: Unpolarized UV emission spectra of Pr:KY<sub>3</sub>F<sub>10</sub>, Pr:YLiF<sub>4</sub>, Pr:BaY<sub>2</sub>F<sub>8</sub>

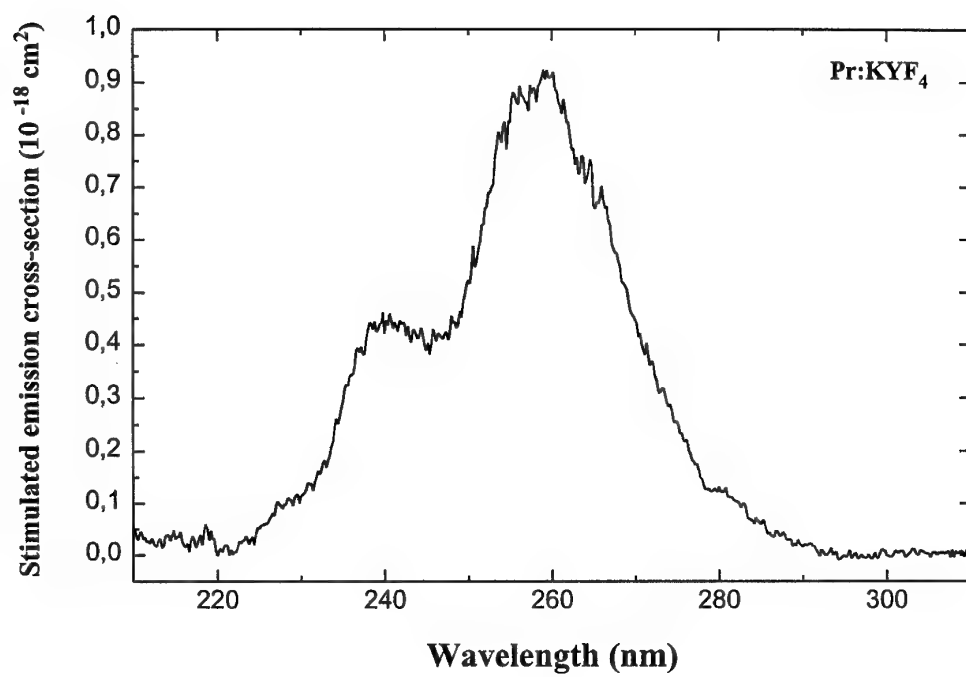


Fig. 7: Unpolarized UV emission spectra of Pr:KYF<sub>4</sub>

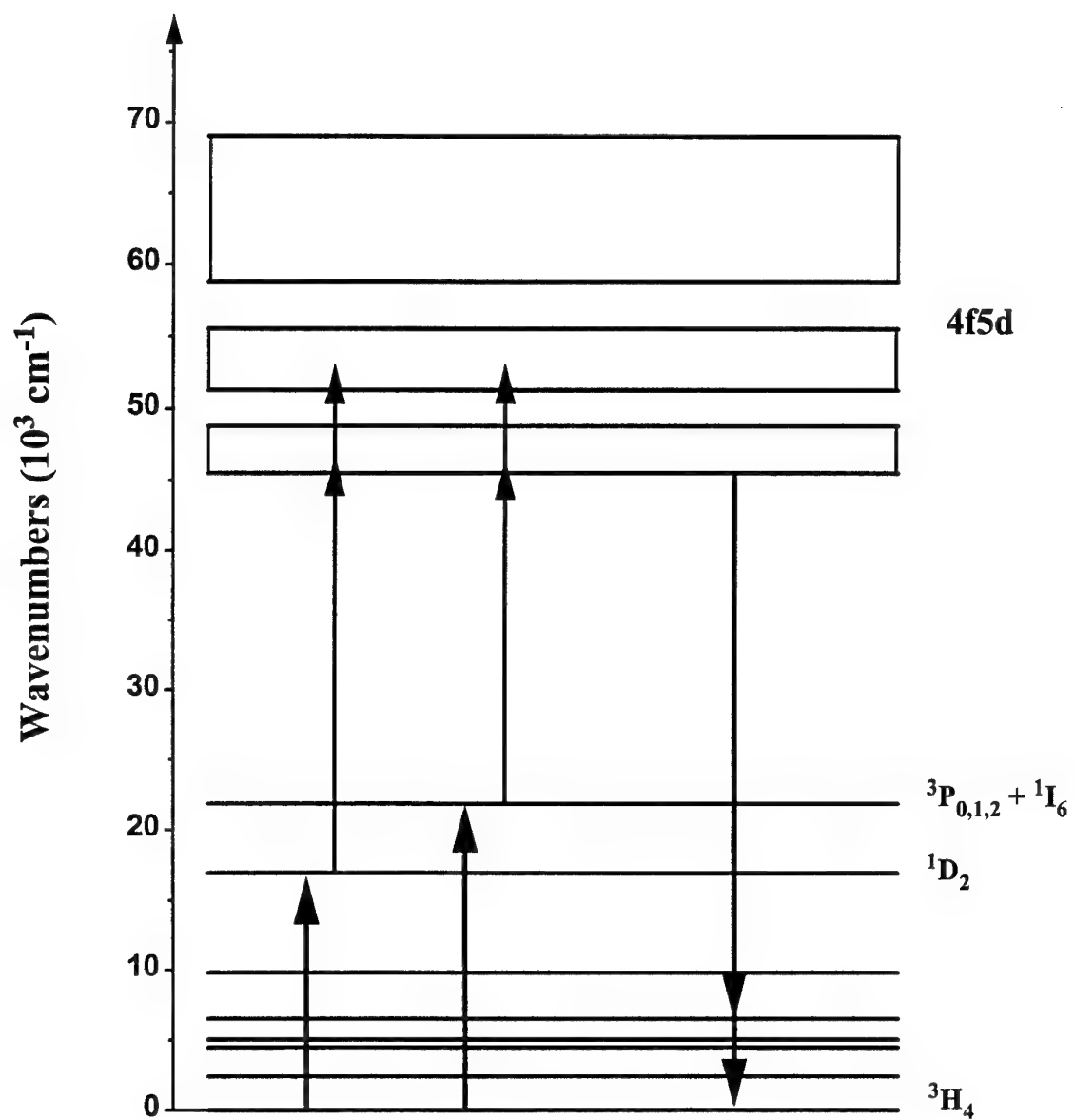


Fig. 8: Energy level scheme for  $\text{Pr}^{3+}$  in  $\text{LiYF}_4$

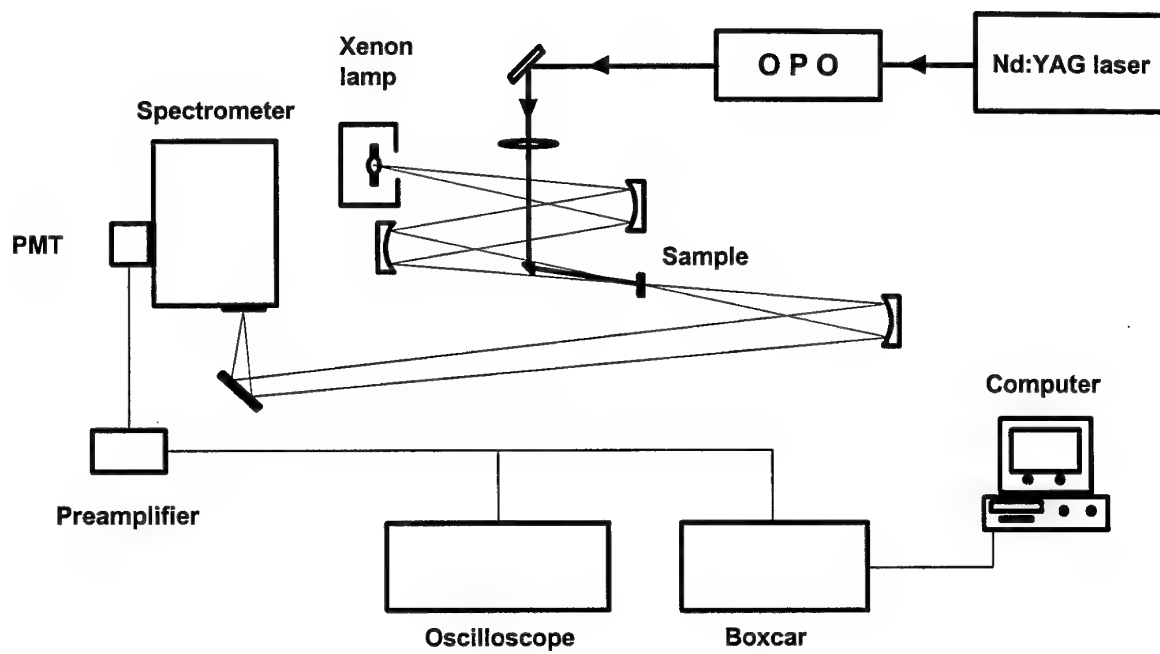


Fig. 9: ESA experimental set-up

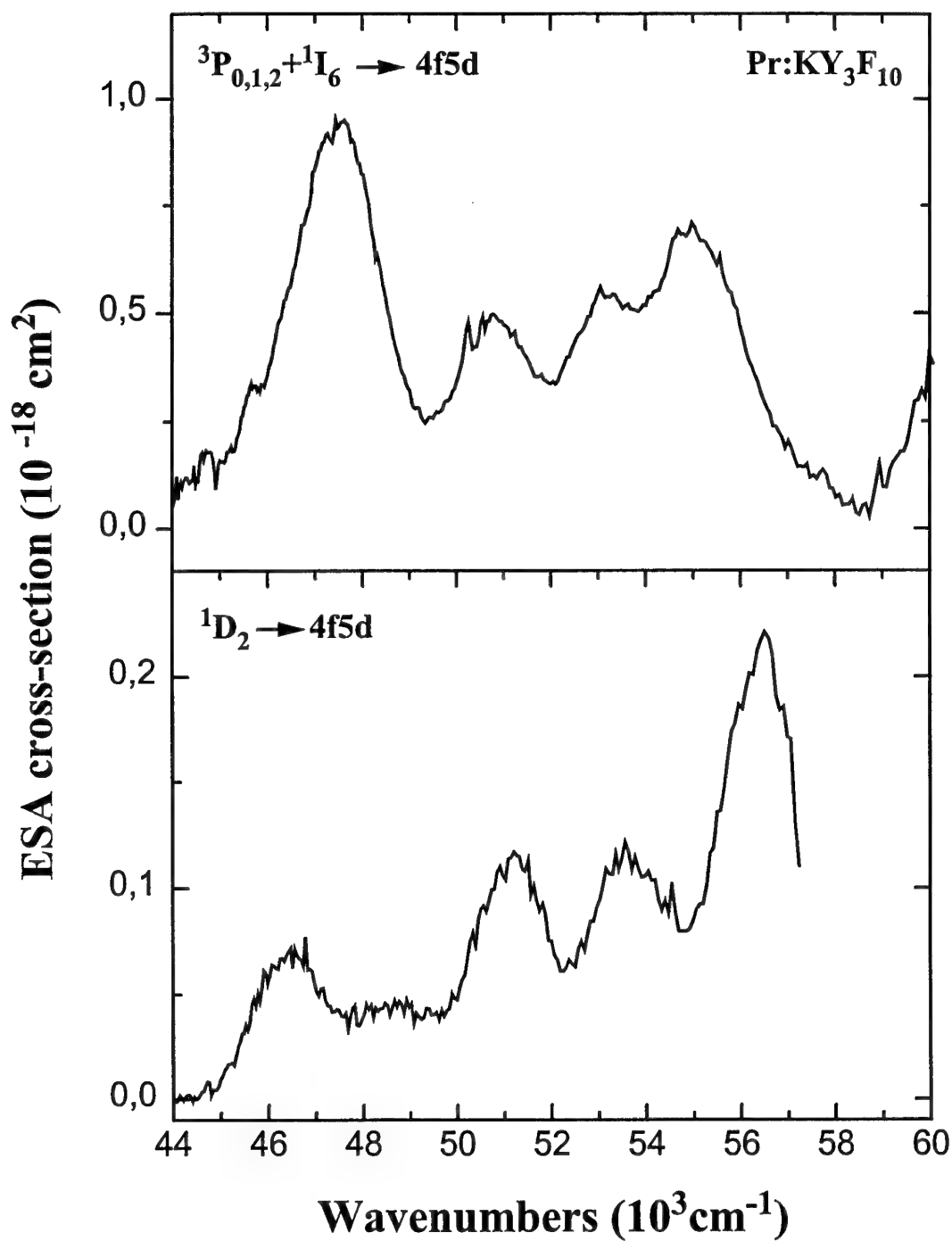


Fig. 10: Excited-state absorption spectra of Pr:KY<sub>3</sub>F<sub>10</sub>, from the  $^1D_2$  and  $^3P_{0,1,2} + ^1I_6$  multiplets

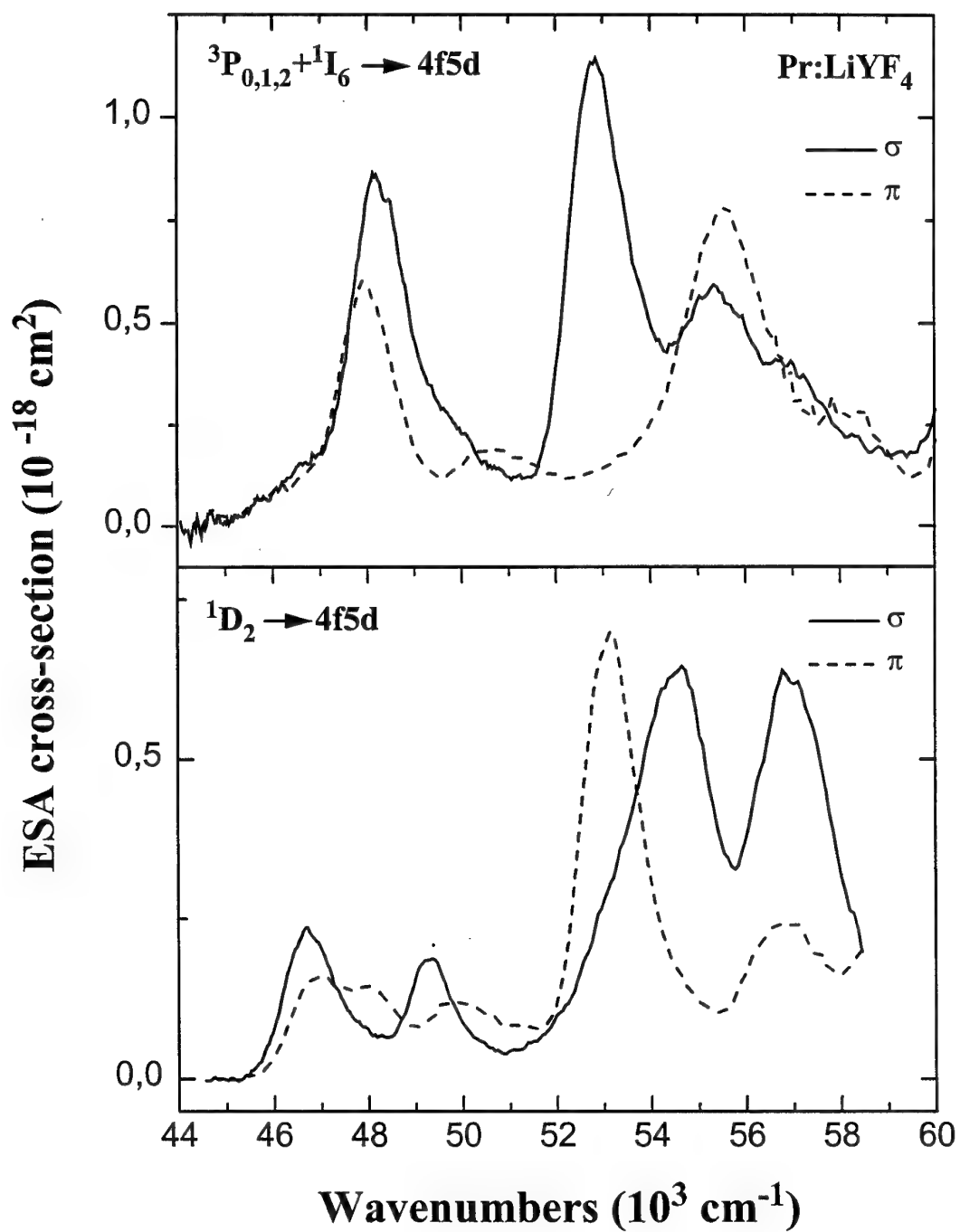


Fig. 11: Polarized excited-state absorption spectra of Pr:YLiF<sub>4</sub>, from the  $^1D_2$  and  $^3P_{0,1,2} + ^1I_6$  multiplets

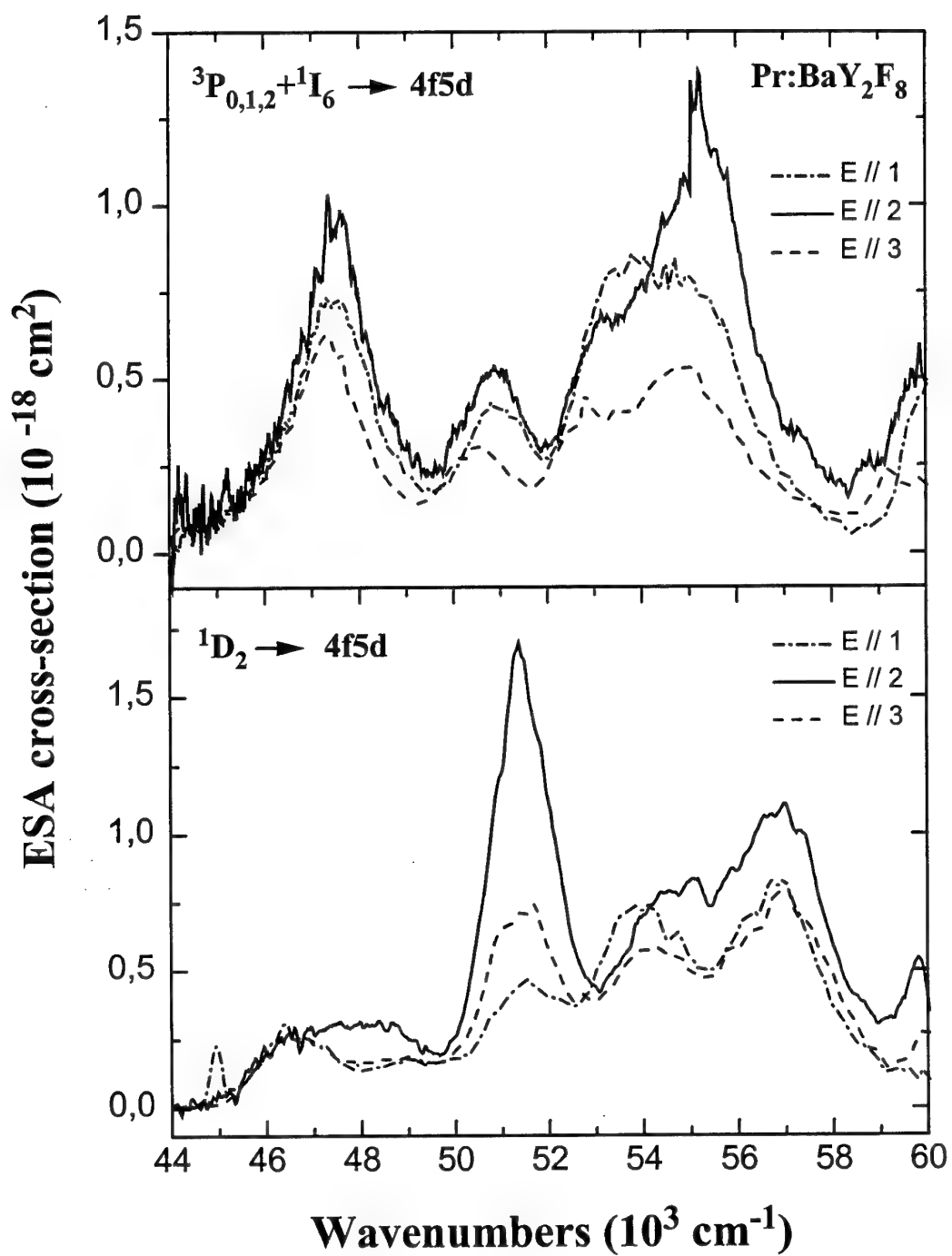


Fig. 12: Polarized excited-state absorption spectra of Pr:BaY<sub>2</sub>F<sub>8</sub>, from the  $^1D_2$  and  $^3P_{0,1,2} + ^1I_6$  multiplets

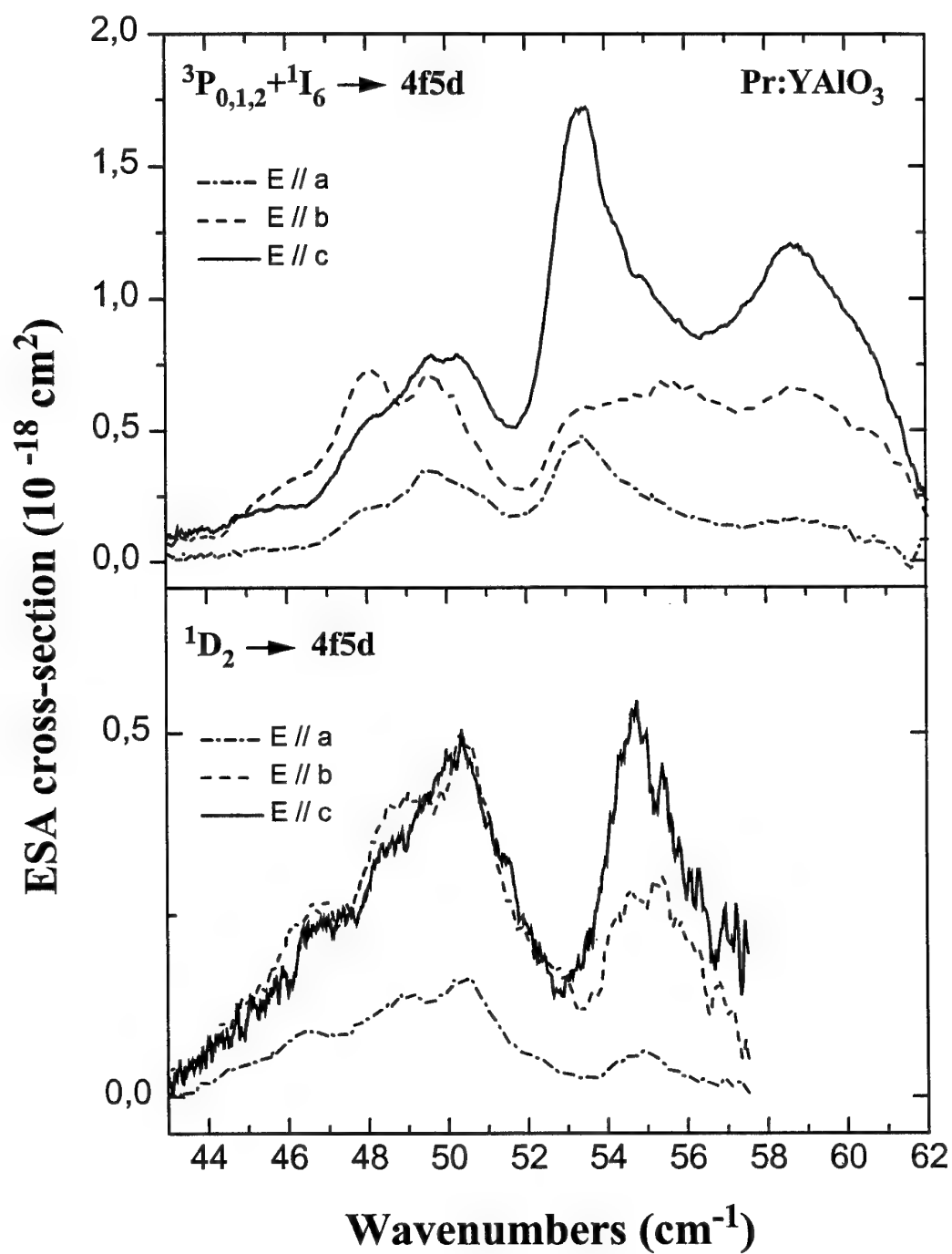


Fig. 13: Polarized excited-state absorption spectra of Pr:YAlO<sub>3</sub>, from the  $^1D_2$  and  $^3P_{0,1,2} + ^1I_6$  multiplets

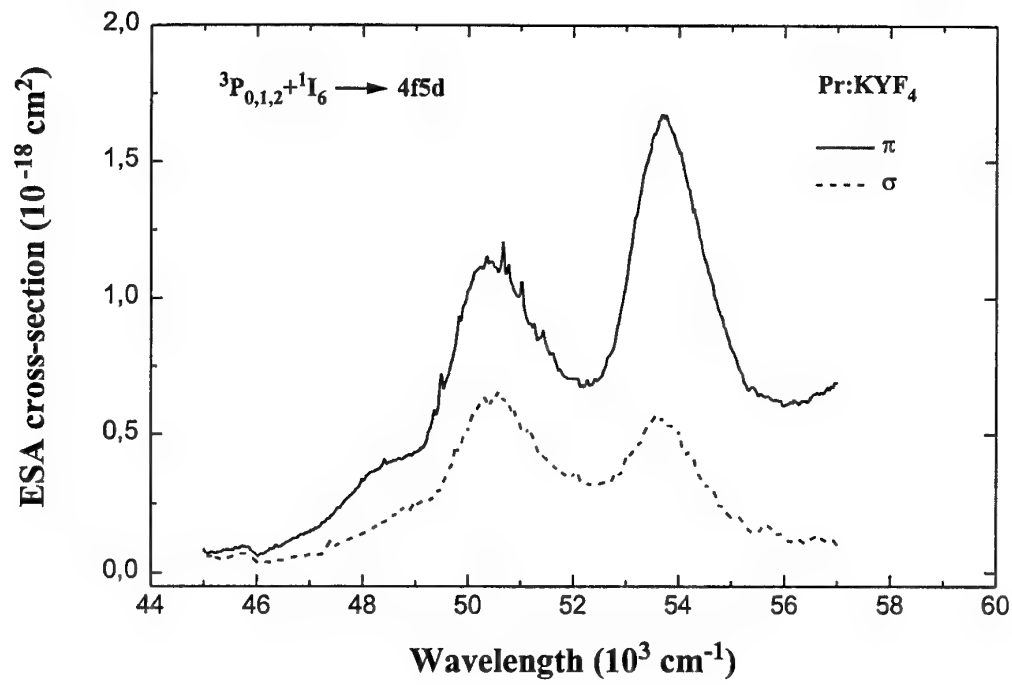


Fig. 14: Polarized excited-state absorption spectra of Pr:KYF<sub>4</sub>, from the  $^3P_{0, 1, 2} + ^1I_6$  multiplets

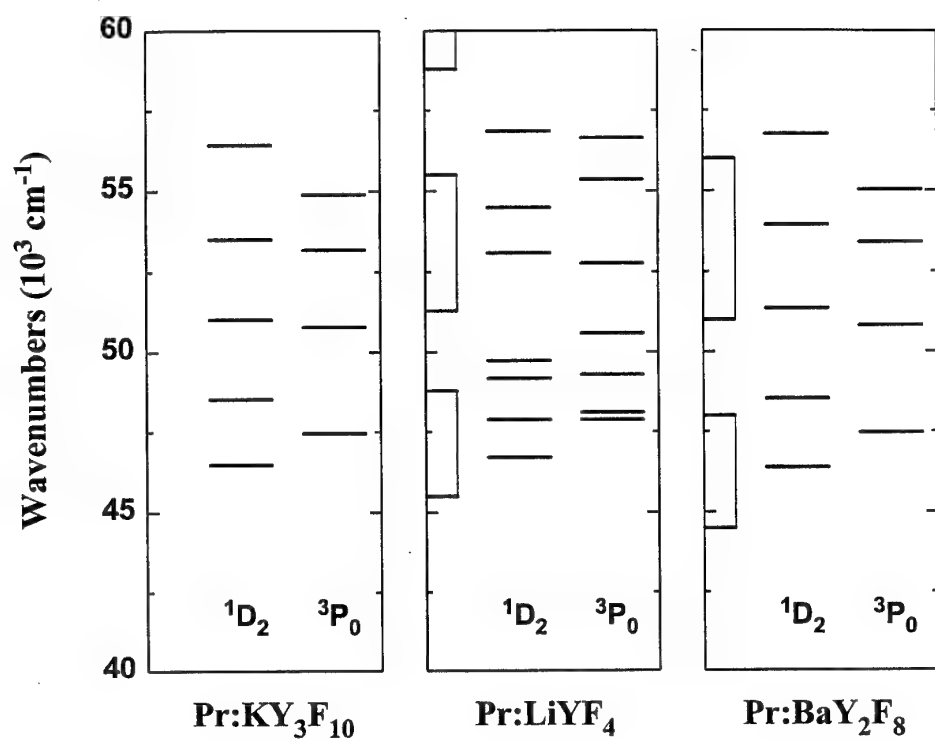


Fig. 15: 4f5d energy levels according to the  $^3H_4 \rightarrow 4f5d$  and the  $^3P_0 \rightarrow 4f5d$  and  $^1D_2 \rightarrow 4f5d$  ESA spectra of Pr:KY<sub>3</sub>F<sub>10</sub>, Pr:LiYF<sub>4</sub> and Pr:BaY<sub>2</sub>F<sub>8</sub>

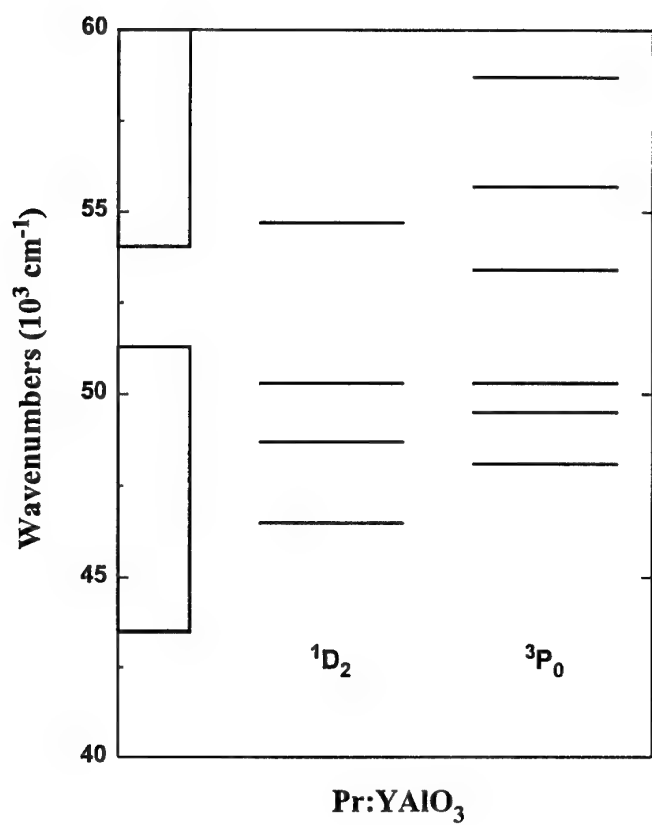


Fig. 16: 4f5d energy levels according to the  $^3\text{H}_4 \rightarrow 4\text{f5d}$  and the  $^3\text{P}_0 \rightarrow 4\text{f5d}$  and  $^1\text{D}_2 \rightarrow 4\text{f5d}$  ESA spectra of Pr:YAlO<sub>3</sub>

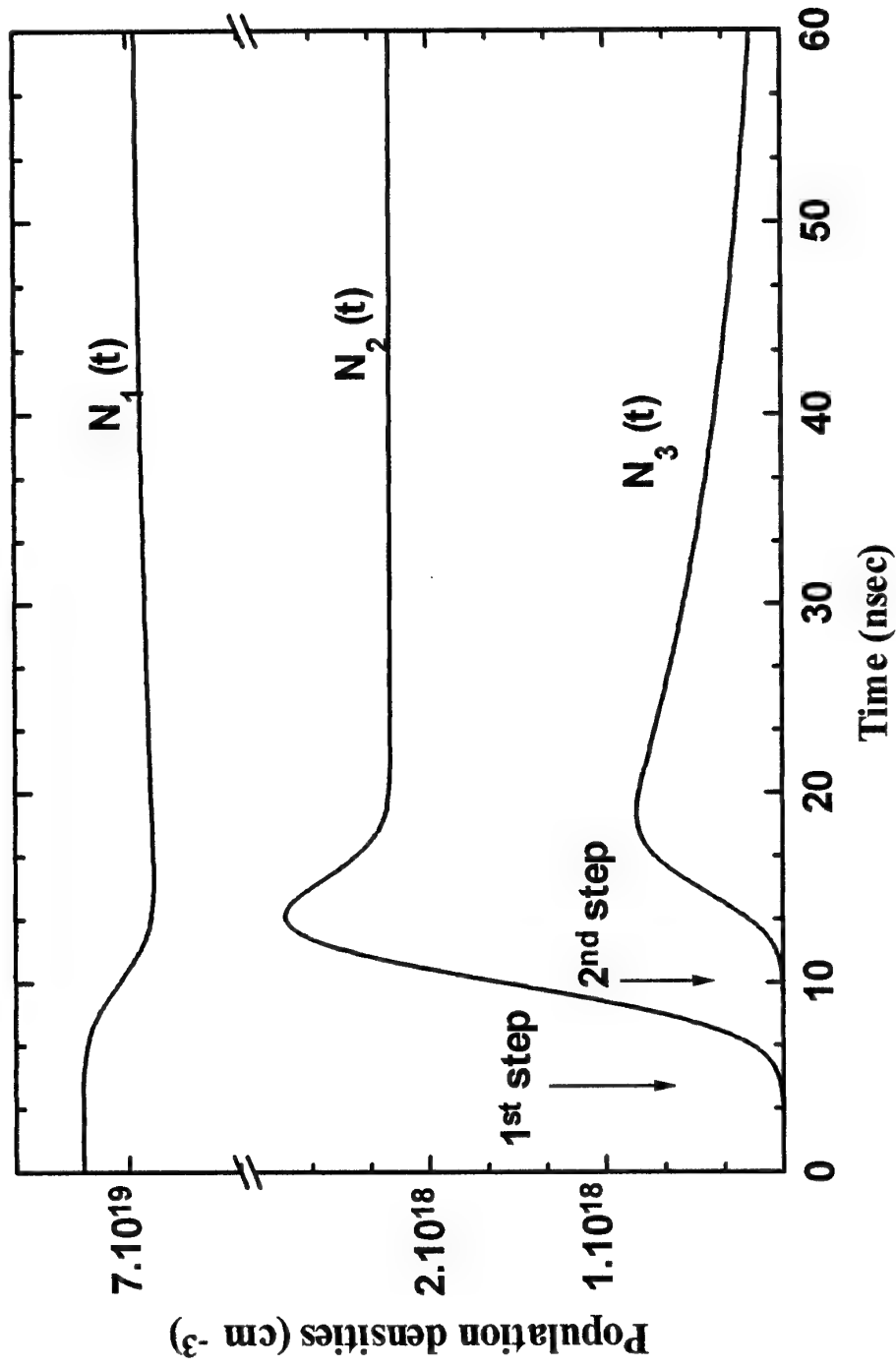


Fig. 17 : Temporal evolutions of the  $^3\text{H}_4$  ground-state,  $^3\text{P}_{0,1,2}$  excited multiplet and  $4f5d$  electronic configuration populations  $N_1$ ,  $N_2$  and  $N_3$  after two-step excitation pumping,

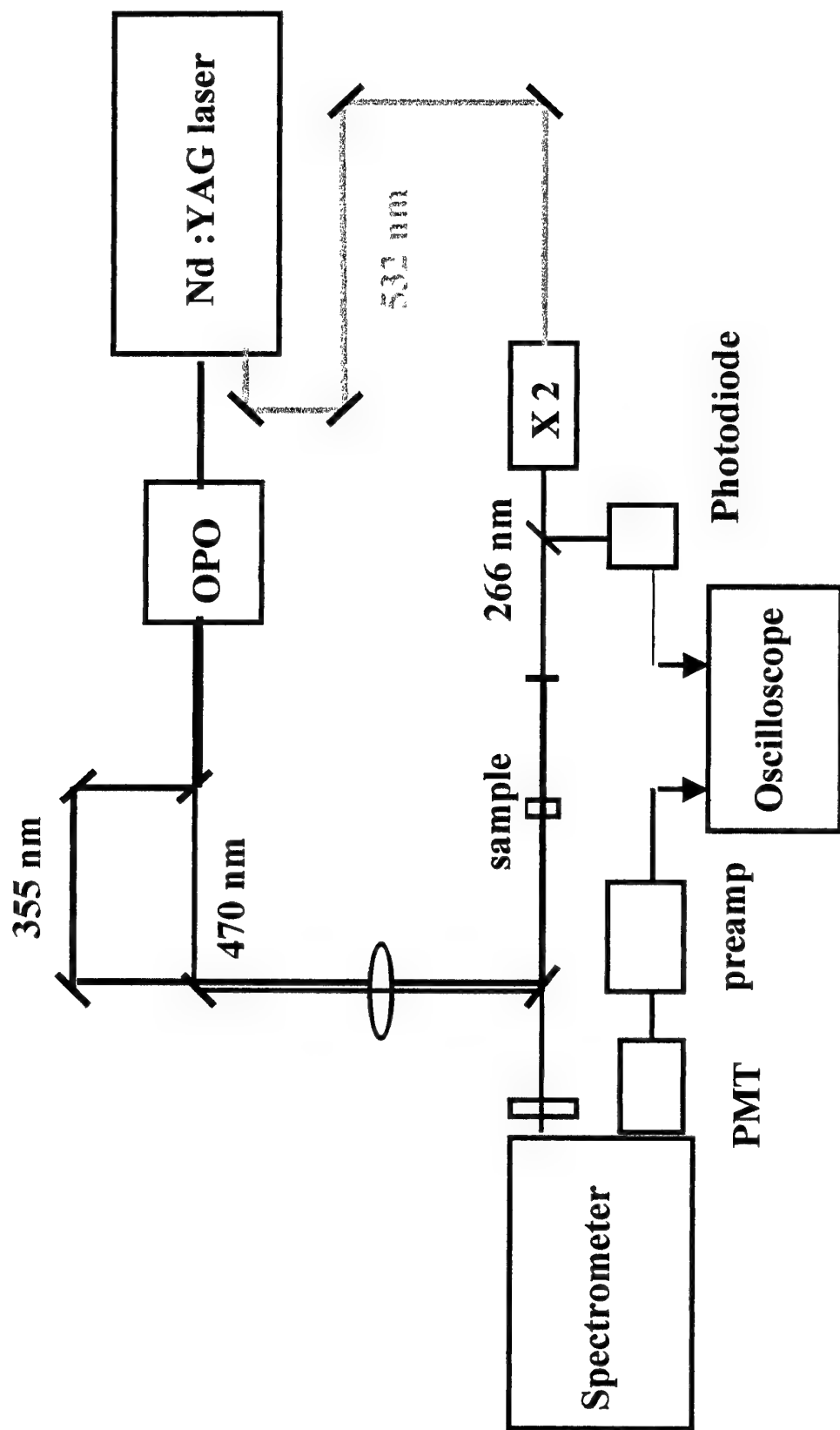


Fig. 18 : Experimental set-up used for measurements of laser gain at 266 nm and solarisation spectra after two-step excitation with 470 and 355 nm pump photons

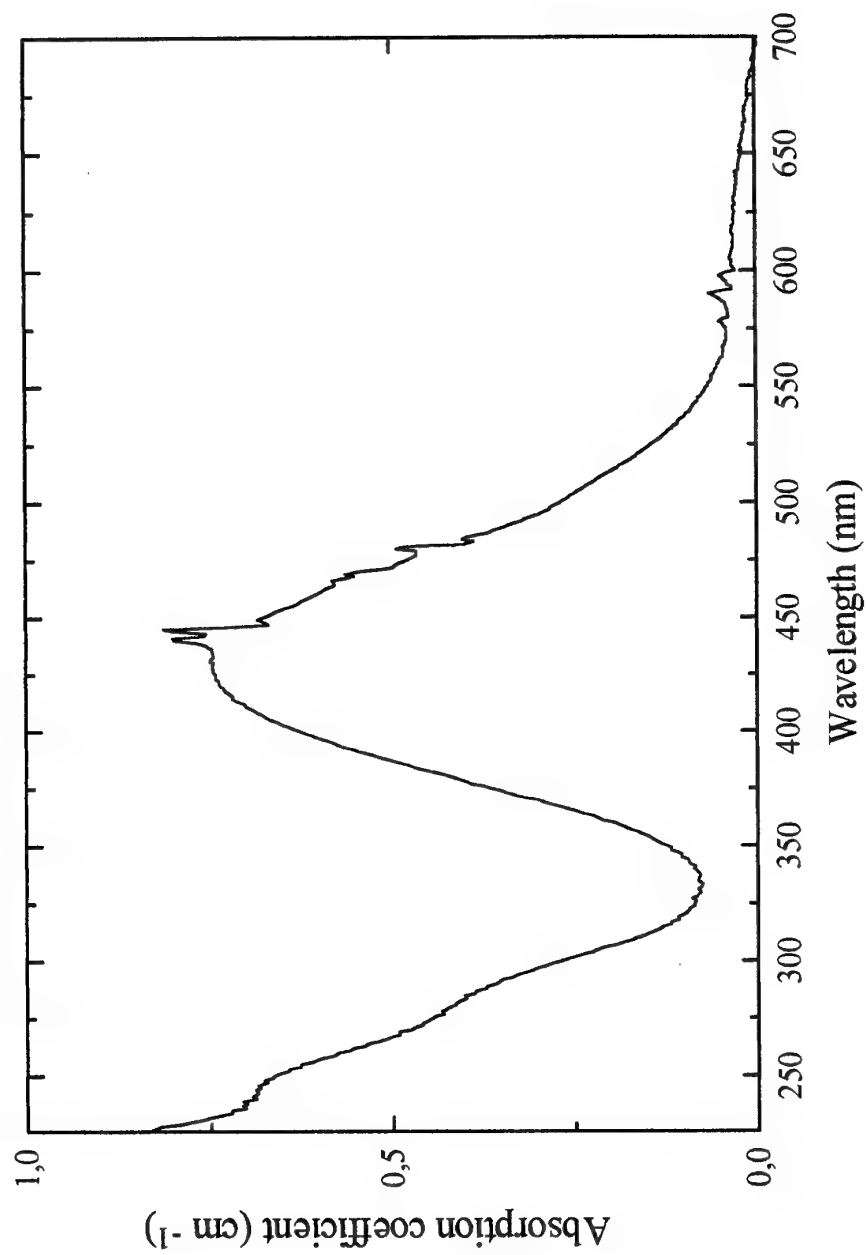


Fig. 19: Solarisation absorption spectrum observed in Pr:KY<sub>3</sub>F<sub>10</sub> after two-step excitation pumping at 470 and 355 nm

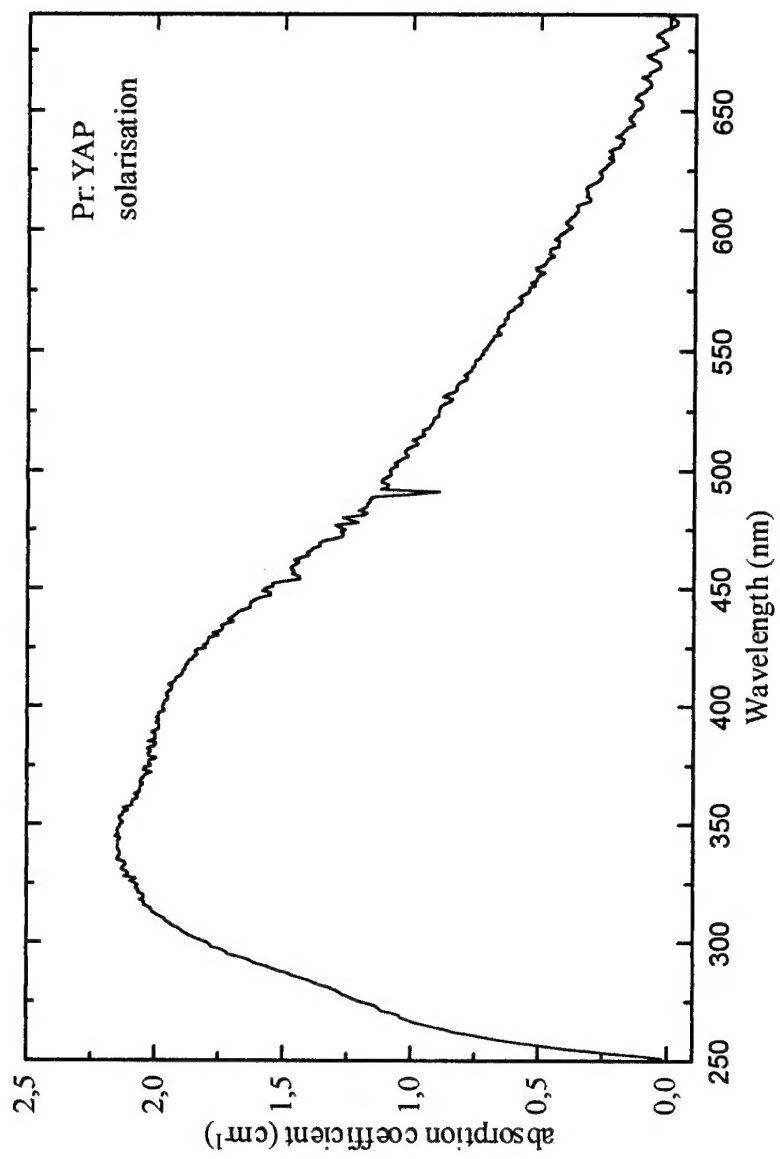


Fig. 20 : Solarisation absorption spectrum observed in Pr :YAlO<sub>3</sub> after two-step excitation pumping at 470 and 355 nm

fig. 21 : Relative positions of the  $\text{Pr}^{3+}$  energy levels and of the valence and conduction bands in various materials

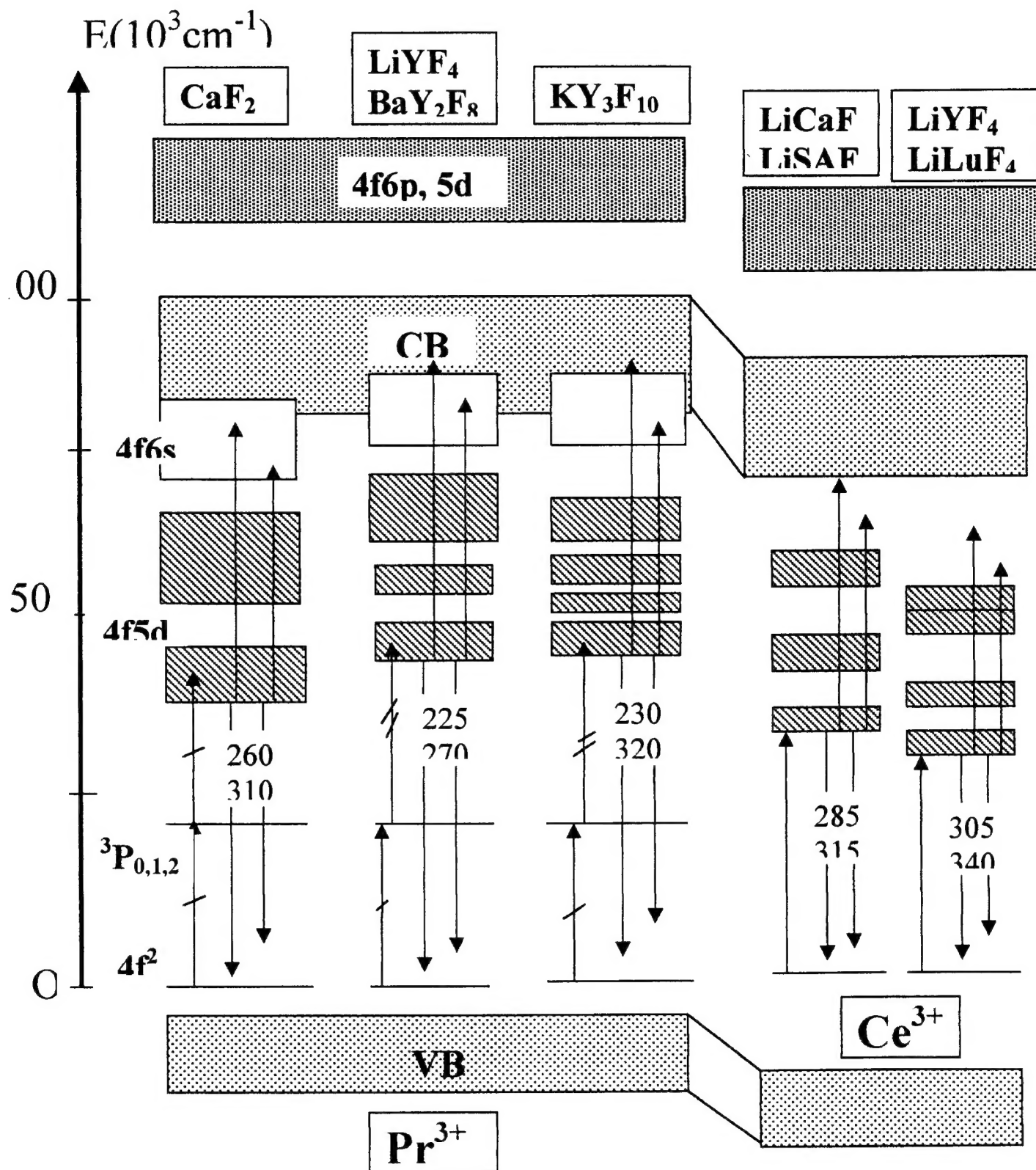


Fig. 22 : Relative positions of the  $\text{Pr}^{3+}$  ion energy levels and of the valence and conduction bands of the materials

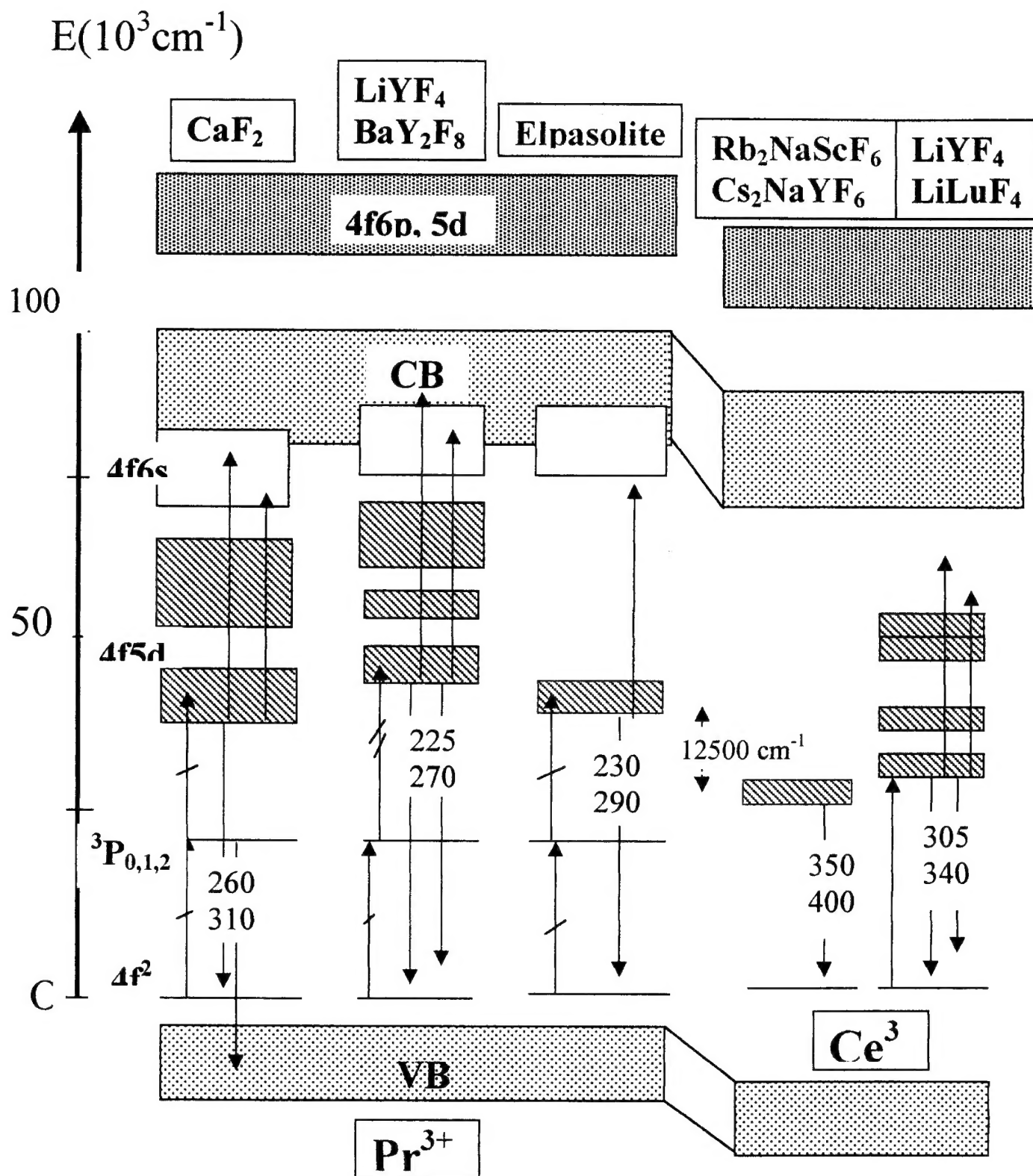


Fig. 23 : Relative positions of the  $\text{Pr}^{3+}$  and  $\text{Nd}^{3+}$  ions energy levels and of the valence and conduction bands of the materials

